NTNU – Trondheim
Norwegian University of
Science and Technology

Calculation of Wave Forces on Structures using REEF3D

Arun Mulky Kamath

Coastal and Marine Civil Engineering
Submission date: June 2012
Supervisor: Hans Sebastian Bihs, BAT
Co-supervisor: Øivind Asgeir Arntsen, BAT

Norwegian University of Science and Technology
Department of Civil and Transport Engineering

ERASMUS MUNDUS MSC PROGRAMME

COASTAL AND MARINE ENGINEERING AND MANAGEMENT
COMEM

WAVE FORCES ON STRUCTURES USING REEF3D

Norwegian University of Science and Technology
11 June 2012

Arun Mulky Kamath
4128796

The Erasmus Mundus MSc Coastal and Marine Engineering and Management is an integrated programme organized by five European partner institutions, coordinated by Delft University of Technology (TU Delft).
The joint study programme of 120 ECTS credits (two years full-time) has been obtained at three of the five CoMEM partner institutions:

- Norges Teknisk- Naturvitenskapelige Universitet (NTNU) Trondheim, Norway
- Technische Universiteit (TU) Delft, The Netherlands
- City University London, Great Britain
- Universitat Politècnica de Catalunya (UPC), Barcelona, Spain
- University of Southampton, Southampton, Great Britain

The first year consists of the first and second semesters of 30 ECTS each, spent at NTNU, Trondheim and Delft University of Technology respectively.
The second year allows for specialization in three subjects and during the third semester courses are taken with a focus on advanced topics in the selected area of specialization:

- Engineering
- Management
- Environment

In the fourth and final semester an MSc project and thesis have to be completed.
The two year CoMEM programme leads to three officially recognized MSc diploma certificates. These will be issued by the three universities which have been attended by the student. The transcripts issued with the MSc Diploma Certificate of each university include grades/marks for each subject. A complete overview of subjects and ECTS credits is included in the Diploma Supplement, as received from the CoMEM coordinating university, Delft University of Technology (TU Delft).

Information regarding the CoMEM programme can be obtained from the programme coordinator and director

Prof. Dr. Ir. Marcel J.F. Stive
Delft University of Technology
Faculty of Civil Engineering and geosciences
P.O. Box 5048
2600 GA Delft
The Netherlands

NORWEGIAN UNIVERSITY OF SCIENCE AND TECHNOLOGY
DEPARTMENT OF CIVIL AND TRANSPORT ENGINEERING

Report Title: Calculation of Wave Forces using REEF3D	Date: 11 June 2012 Number of pages (incl. appendices): 86			
	Master Thesis	x	Project Work	

Name:
Arun Mulky Kamath

Professor in charge/supervisor:
Hans Bihs

Other external professional contacts/supervisors: -

Abstract:

The objective of this study is to explore a good alternative to physical modelling in marine civil engineering by testing the numerical wave tank feature of the open source Computational Fluid Dynamics (CFD) package, REEF3D. The two tasks set to achieve this objective: first validate the numerical wave tank and test its performance under different numerical and wave parameters. Second to use the wave tank to calculate wave forces on a structure and validate the numerical solution.

This work is limited to calculating a simple case of non-breaking wave forces on a single cylindrical pile placed in a regular wave field, as CFD is a resource intensive method and running more complex cases would require more time both in terms of man hours for coding and testing of the package and computational time to carry out the numerical experiment.

The validation of the numerical wave tank is carried out by comparing the numerical results generated with the analytical values obtained using wave theory. Various parameters like grid cell density, time step size, numerical beach width, relaxation methods for wave generation and absorption and discretization schemes are tested. In addition, the performance of the wave tank at different amplitudes and wave types is observed. To validate the wave forces calculated by the model, the theoretical force acting on the pile is calculated using the Morison formula and compared with the numerical solution obtained.

The wave tank produces good results with a wave amplitude error of 0.24% for a fifth order Stokes wave of 0.05m amplitude and 2m wavelength at a grid cell density of 100 cells per wavelength, Courant-Friedrich-Lewy number 0.1 and numerical beach width of 4m using the WENO scheme for spatial discretization and 4^{th} order Runge-Kutta method for time discretization.
Wave forces calculated in the wave tank slightly is under estimated compared to the values obtained theoretically using the Morison equation, for four numerical experiments carried out in the study.

Keywords:

1. wave forces
2. REEF3D
3. numerical wave tank
4. cylindrical pile

NTNU
Fakultet for ingeniørvitenskap og teknologi
Institutt for bygg, anlegg og transport

MASTER DEGREE THESIS

Spring 2012
for

Student: Arun Mulky Kamath

Wave Forces on Structures using REEF3D

BACKGROUND

This thesis work sets out to explore the application of Computational Fluid Dynamics (CFD) in the field of marine civil engineering. The aim of this study is to validate a numerical wave tank and test its performance under different numerical and wave parameters and use it to calculate non-breaking wave forces on a cylindrical pile and validate the numerical result obtained.

In the age of growing computing power, a good alternative to laboratory testing is the use of numerical simulations. Numerical modelling allows for testing on the real world scale, in comparison to the scaled down versions that have to be used in the wave flume. This can provide a greater detail of the phenomena that take place during the action of waves on a structure. In addition, a numerical wave tank offers more flexibility in terms of parameters that can be chosen for conducting experiments. Full scaled, three dimensional perspective of the interactions can be obtained using a 3-dimensional numerical simulation, which is a product of the vast field called CFD.

TASK DESCRIPTION

First, the numerical wave tank in the program is to be validated for wave generation at the inlet, propagation in the working zone of the wave tank and dissipation at the numerical beach. The effect of the varying computational parameters like the grid density and time step size is to be observed. In addition, performance of the wave tank for various wave types, different wave amplitudes and under many discretization schemes is to be explored. Finally, the model is to be used to determine non-breaking wave forces on a vertical pile.
The results will be compared with available experimental data from literature and the analytical formulae.

General about content, work and presentation

The text for the master thesis is meant as a framework for the work of the candidate. Adjustments might be done as the work progresses. Tentative changes must be done in cooperation and agreement with the professor in charge at the Department.

In the evaluation thoroughness in the work will be emphasized, as will be documentation of independence in assessments and conclusions. Furthermore the presentation (report) should be well organized and edited; providing clear, precise and orderly descriptions without being unnecessary voluminous.

The report shallinclude:

- Standard report front page (from DAIM, http://daim.idi.ntnu.no/)
- Title page with abstract and keywords.(template on:http://www.ntnu.no/bat/skjemabank)
- Preface
- Summary and acknowledgement. The summary shall include the objectives of the work, explain how the work has been conducted, present the main results achieved and give the main conclusions of the work.
- Table of content including list of figures, tables, enclosures and appendices.
- If useful and applicable a list explaining important terms and abbreviations should be included.
- The maintext.
- Clear and complete references to material used, both in text and figures/tables. This also applies for personal and/or oral communication and information.
- Text of the Thesis (these pages) signed by professor in charge as Attachment 1..
- The report musts have a complete page numbering.

Advice and guidelines for writing of the report is given in: “Writing Reports” by Øivind Arntsen. Additional information on report writing is found in “Råd og retningslinjer for rapportskriving ved prosjekt og masteroppgave ved Institutt for bygg, anlegg og transport” (In Norwegian). Both are posted postedon http://www.ntnu.no/bat/skjemabank

Submission procedure

Proceduresrelating to the submissionof the thesis aredescribedin DAIM (http://daim.idi.ntnu.no/). Printing of the thesis is ordered through DAIM directly to Skipnes Printing delivering the printed paper to the department office 2-4 days later. The department will pay for 3copies, of which the institute retains two copies. Additional copies must be paid for by the candidate/ external partner.

On submission of the thesis the candidate shall submit a CD with the paper in digital form in pdf and Word version, the underlying material (such as data collection)in digital form (eg. Excel). Students must submit the submission form (fromDAIM) where both the Ark-BiblinSBI and Public Services (Building Safety) of SBII has signed the form. The submission form including the appropriate signatures must be signed by the department office before the form is delivered Faculty Office.

Documentation collected during the work, with support from the Department, shall be handed in to the Department together with the report.

According to the current laws and regulations at NTNU, the report is the property of NTNU. The report and associated results can only be used following approval from NTNU (and external cooperation partner if applicable). The Department has the right to make use of the results from the work as if conducted by a Department employee, as long as other arrangements are not agreed upon beforehand.

Tentative agreement on external supervision, work outside NTNU, economic support etc.
Separate description to be developed, if and when applicable. See http://www.ntnu.no/bat/skjemabank for agreement forms.

Health, environment and safety (HSE)http://www.ntnu.edu/hse
NTNU emphasizes the safety for the individual employee and student. The individual safety shall be in the forefront and no one shall take unnecessary chances in carrying out the work. In particular, if the student is to participate in field work, visits, field courses, excursions etc. during the Master Thesis work, he/she shall make himself/herself familiar with " Fieldwork HSE Guidelines". The document is found on the NTNU HMS-pages athttp://www.ntnu.no/hms/retningslinjer/HMSR07E.pdf

The students do not have a full insurance coverage as a student at NTNU. If you as a student want the same insurance coverage as the employees at the university, you must take out individual travel and personal injury insurance.

Start and submission deadlines
The work on the Master Thesis starts on January 16, 2012

The thesis report as described above shall be submitted digitally in DAIM at the latest at 3pm June 11, 2012

Professor in charge: Hans Bihs

Trondheim, January 16, 2012.

_____
Professor in charge (sign)

Abstract

The objective of this study is to explore a good alternative to physical modelling in marine civil engineering by testing the numerical wave tank feature of the open source Computational Fluid Dynamics(CFD) package, REEF3D. The two tasks set to achieve this objective: First validate the numerical wave tank and test its performance under different numerical and wave parameters. Second to use the wave tank to calculate wave forces on a structure and validate the numerical solution.
This work is limited to calculating a simple case of non-breaking wave forces on a single cylindrical pile placed in a regular wave field, as CFD is a resource intensive method and running more complex cases would require more time both in terms of man hours for coding and testing of the package and computational time to carry out the numerical experiment.
The validation of the numerical wave tank is carried out by comparing the numerical results generated with the analytical values obtained using wave theory. Various parameters like grid cell density, time step size, numerical beach width, relaxation methods for wave generation and absorption and discretization schemes are tested. In addition, the performance of the wave tank at different amplitudes and wave types is observed. To validate the wave forces calculated by the model, the theoretical force acting on the pile is calculated using the Morison formula and compared with the numerical solution obtained.
The wave tank produces good results with a wave amplitude error of 0.24% for a fifth order Stokes wave of 0.05m amplitude and 2m wavelength at a grid cell density of 100 cells per wavelength, Courant-Friedrich-Lewy number 0.1 and numerical beach width of 4m using the WENO scheme for spatial discretization and 4^{th} order Runge-Kutta method for time discretization.
Wave forces calculated in the wave tank slightly is under estimated compared to the values obtained theoretically using the Morison equation, for four numerical experiments carried out in the study.

The study concludes that REEF3D is a capable tool for application of CFD methods in the field of marine civil engineering. The results obtained from the validation of the wave tank show promise in this regard. The validation of the wave forces calculated using the model could not be deemed to be conclusive and further study is suggested. Due to the absence of data from simple experiments on wave force on a single cylindrical pile and time constraints, validation was limited to comparison against the Morison formula.

Acknowledgments

This thesis work draws the curtains on my participation as a graduate student in the two year mobility programme−the Erasmus Mundus Masters Course : Coastal and Marine Engineering and Management (CoMEM) of which I am proud to have been a part of and honoured to have been accepted into. I am thankful to the powers that be that resulted in my enrollment with the financial assistance of the Education, Audio-Visual and Culture Executive Agency (EACEA) of the European Commission.
I am also grateful to Associate Professor Øivind Arntsen for bringing to my knowledge the availability of a master thesis task involving Computational Fluid Dynamics at the Department of Civil and Transport Engineering (BAT), Norwegian University of Science and Technology (NTNU). I am thankful to him for providing me with the opportunity to work on this topic.
In the words of Nobel laureate Anatole France, "Nine-tenths of education is encouragement". I would like to express my wholehearted thanks to Adj. Associate Professor Hans Bihs, under whose supervision this thesis work has been carried out. Without his support, guidance, insights and encouragement, it would have been a herculean task to carry out this study.
Discussions about REEF3D with PhD stipendiat A.C.Mayilvahanan helped me to understand my work better and also spot my mistakes in time. Also, I was lucky to have had my classmate Tedy Asyikin to compare with and rightly pace my work and have a listening ear during the drag and turbulent phases of the work. From across the seas, Ir. Mohammed Aslam took the time to patiently proof read the thesis. Special thanks to all of them who made this research work a happier journey.
Finally, I would like to thank my officemate Ir.Loup Thauvin, friends Ir. Mrinal Shenoy and Ir. Gurvinder Singh and also Hans for their help in compiling this document using LaTeX.

Contents

List of Figures

List of Symbols

λ	Wavelength
D	Diameter
ρ	Density
t	Time
∇	Divergence operator
U	Velocity
$_{i,\ j,\ k}$	Vectors along the x, y and z-axes
μ	Fluid viscosity (dynamic)
P	Pressure
g	Acceleration due to gravity
ϕ	Level set function
$_i$ *(in numerical schemes)*	Time step of iteration
$\omega_1,\ \omega_2,\ \omega_3$	WENO stencil weights
$\alpha_1,\ \alpha_2,\ \alpha_3$	WENO stencil weight determiner
$IS_1,\ IS_2,\ IS_3$	WENO stencil smoothness indicators
L()	Spatial discretization of the function
C	Courant Number
ν	Fluid viscosity(kinematic)
ν_t	Eddy viscosity
V	Maximum viscosity
S_{max}	Source term contribution from surface and volume forces
U^*	Intermediate velocity
k	Turbulent kinetic energy
ω	Specific turbulent dissipation
$c_\mu,\ c_{\omega 1},\ c_{\omega 2},\ \sigma_k,\ \sigma_\omega$	Closure coefficients
S_{ij}	Strain tensor
U^+	Dimensionless wall velocity
κ	constant = 0.4
d	Water depth
k_s	Equivalent sand roughness

Δy_p	Distance from the wall to cell centre
ϵ_{wall}	Mean wall thickness
τ_ω	Wall shear stress
2ϵ	Transition zone thickness
$S(\phi)$	Smooth signed distance function
Φ	Velocity potential
$\Psi(x)$	Relaxation function
^{p}	Steepness exponent
η	Free surface elevation
ω_f	Wave angular frequency
k_f	Wave number
a	Wave amplitude
C	Wave celerity
H	Wave height
z	Height to the free surface from bed
θ	Wave phase
ϵ^n	Perturbation factor
dx	Grid cell width
KC	Keulegan-Carpenter number
T	Wave period
S_0	Strouhal number
f_0	Vortex shedding frequency
f_{FK}	Froude-Krylov force
π	Mathematical constant, $\frac{22}{7}$
$\dot{U}$	Particle acceleration
f_d	Drag force
C_d	Drag force coefficient
Re	Reynolds number
f	Force
C_a	Added mass coefficient
C_m	Inertia force coefficient
Γ	Surface vector
$\mathbf{n}$	Surface normal vector
τ	Shear stress
R^2	Coefficient of determination

Chapter 1

Introduction

1.1 Computational Fluid Dynamics in marine civil engineering

Marine hydrodynamics mainly deals with the interaction between waves and marine structures. In the course of studying this phenomenon, the characterization of the sea state parameters poses a challenge due to the random nature of the sea state. Many theories have been proposed to understand and analytically represent water waves, starting from the linear wave theory to Stokes' -second, -third, -fifth order theories, cnoidal theory and so on. They are used to generate waves in laboratory wave flumes to create a simplified representation in form of a regular wave field to understand the interaction of waves with marine structures. It has to be noted, though, that the waves used for studies in experiments are generally unidirectional and regular, whereas in the field, the random nature of the sea state gives rise to a much more complex wave field. In addition to the aforementioned problem, the other obstacle in understanding wave-structure interactions is the complexity of the fluid dynamics involved. According to Sarpkaya [26], the current analytical, experimental, and operational knowledge is still insufficient to describe the complexities of fluid loading and dynamic response of offshore structures accurately. Physical modelling has been applied to simulate the field phenomena in order to aid in the design of marine structures which can withstand a certain set of design parameters.
In the age of growing computing power, a good alternative to laboratory testing is the use of numerical simulations. Numerical modelling allows for testing on the real world scale, in comparison to the scaled down versions that have to be used in the wave flume. This can provide a greater detail of the phenomena that take place during the action of waves on a structure. In addition, a numerical wave tank offers more flexibility in terms of parameters that can be chosen for conducting experiments. Full scaled, three dimensional perspective of the interactions can be obtained using

a 3-dimensional numerical simulation, which is a product of the vast field called Computational Fluid Dynamics (CFD).
Wave forces on structures have been analytically evaluated, so far, using the potential theory and the Morison formula. Morison formula is preferred in cases where there is flow separation. A general definition of the conditions under which these equations are valid is difficult to arrive at; like a criteria based on the ratio λ/D can be incorrect, as described by Moe and Gudmestad [23]. Also, the inertia and drag coefficients used to determine the forces are based on empirical data.
In this scenario, it is beneficial to adopt numerical simulations to evaluate wave forces on marine structures. Accurate numerical simulations provide great insight into the physical processes which could not be attained through an experimental approach[22]. The current state of computational power and expected future advances make it possible to employ three dimensional numerical simulations in fluid dynamics and obtain results in a reasonable amount of time.
Various commercial software like Star CCM+, Ansys Fluent and open source software like REEF3D, OpenFOAM are available, to name a few, for the purpose of employing numerical simulations to solve engineering problems. A point to be noted though is that most of the programs available currently were not built specifically to cater to the simulation of marine and coastal engineering free surface flows. REEF3D was initially developed to evaluate local scouring in open channel flows[4] and is well suited to cater to simulation of water waves.

1.2 Objectives of the study

The objective of this study is to utilize the open source CFD program, REEF3D, to compute wave forces on marine structures, with a focus on vertical piles. The aim is to be able to realistically visualize wave interaction with a cylindrical pile. To achieve a photo realistic imagery of the free surface, the air-water interface is followed using the level set method to calculate the interface in great detail.
First, the numerical wave tank in the program is to be validated for wave generation at the inlet, propagation in the working zone of the wave tank and dissipation at the numerical beach. The effect of the varying computational parameters like the grid density and time step size is to be observed. In addition, performance of the wave tank for various wave types, different wave amplitudes and under many discretization schemes is to be explored. Finally, the model is to be used to determine non-breaking wave forces on a vertical pile. The results will be compared with available experimental data from literature and the analytical formulae.

1.3 Limitations of the study

The main attraction of CFD is that it incorporates more physics in its calculations with lesser amount of simplification in comparison to other tools like, say, a wave model. It also provides more detailed description of the flow phenomena. But, these features also give it a disadvantage in terms of making it a resource intensive environment. Numerical modelling using CFD requires a large amount of computational power and time. Due to this fact, the focus of the current study is to a simulate a simple case of calculating non-breaking wave force on a single cylindrical pile placed in a regular uni-directional wave field after the validation of the numerical wave tank. Validation of the wave forces against experimental data could prove to be difficult because of the following reasons. First, comparison of the numerical results to the experimental data would require the numerical wave tank to very closely mimic the experimental conditions. In addition, reliable, published physical experiments generally deal with more complicated scenarios than that is visualized to be carried out in the numerical wave tank.

Chapter 2

Numerical Model

This chapter briefly deals with the basic concepts of CFD and the computational methods employed in REEF3D, the CFD software to be used in this study.

2.1 Governing Equations

CFD works on a set of conservation laws. Conservation of a quantity implies that the total amount of the quantity exiting a predefined system is equal to the sum of the amount of the quantity entering and amount of the quantity produced/consumed in the system. The fluid properties to which the laws are applicable are− Mass and Momentum. It is to be noted that momentum conservation leads to the governing equation in fluid dynamics- the Navier Stokes equation. To analytically solve these equations, a reasonable and simplifying assumption of an incompressible fluid is constructed. The implication of the assumption is that the fluid retains its density at all times and thus occupies the same volume throughout the period of observation. This assumption is considered reasonable, as the velocities of air and water in the cases that are to be analyzed in this study, are small enough to be consider the fluids to be incompressible.

- Conservation of Mass:
  The equation for conservation of mass is given by

$$\frac{\partial \rho}{\partial t} + \nabla.(\rho\, U) = 0 \tag{2.1}$$

  With the assumption of incompressibility, the density does not change with space or time. Thus, the term with the derivative of the density disappears and the equation for incompressible flows reduces to

$$\frac{\partial U_i}{\partial x_i} = 0 \tag{2.2}$$

This equation is also known as the equation of continuity.

- Conservation of Momentum:
  The momentum conservation arises from Newton's second law, which states that the rate of change of linear momentum is directly proportional to the sum of the forces acting on the body, in this case, the fluid. The momentum equation here can be written as

$$\frac{\partial U_i}{\partial t} + \frac{\partial U_i U_j}{\partial x_j} = \frac{\partial}{\partial x_j}\left(\mu \frac{\partial u_i}{\partial x_j}\right) - \frac{1}{\rho}\frac{\partial P}{\partial x_i} \tag{2.3}$$

  Using the equation of continuity 2.2 with the above equation, the Navier Stokes equation can be formed and is written as

$$\frac{\partial U_i}{\partial t} + U_j \frac{\partial U_i}{\partial x_j} = -\frac{1}{\rho}\frac{\partial P}{\partial x_i} + \frac{\partial}{\partial x_j}\left[\nu\left(\frac{\partial U_i}{\partial x_j} + \frac{\partial U_j}{\partial x_i}\right)\right] + g_i \tag{2.4}$$

2.2 Numerical Treatment of Governing Equations

A fluid flow problem is numerically resolved by the application of numerical methods. The first step towards the application of these methods is the discretization of the governing equations. This means expression of a continuous equation in a form that is applicable to a finite domain. The method of finite differences is one of the methods that can be used to discretize the equations and is the one that is employed in this study. Other methods that can be used for this purpose are the method of finite elements and the method of finite volumes. These methods are not a part of this work and shall not be discussed further.

A computational domain can be defined as a set of points on a line, for a one dimensional case, a set of points on a mesh for a two dimensional case and a set of points on a three dimensional grid for 3-dimensional computation. The process of defining discrete points over a continuous domain for the purpose of evaluating a process numerically is called spatial discretization. The set of points so generated is referred to as the grid. In this study, a Cartesian staggered grid is utilized for spatial discretization.

A staggered grid is a grid on which the unknown variables are not located at the same grid points. For example, the velocities are located on the midpoints of the cell edges and the pressure at the centre of the grid. This is contrary to another arrangement called the colocated grid, where all the variables are defined at the cell edges. The main advantage of the staggered grid arrangement is that it prevents the pressure oscillations which could occur if all the variables were defined at the cell edges as in a colocated grid arrangement. A Cartesian grid is a grid where the points are even placed across the domain forming congruent parallelotopes or 'bricks'.

Numerical approximations have two characteristics which determine the applicability of the particular scheme to a particular scenario:

- Accuracy: This is determined by the order of the truncation error. The truncation error is the difference between the exact solution and the numerical approximation. The order is determined by the order of the expression obtained after applying Taylor expansion to the governing differential equation. The scheme is said to be consistent when the error tends to zero as the grid or step size approaches zero. Thus, for a consistent scheme, higher the order of the error term, higher the accuracy obtained by improving the resolution of the grid.
- Stability: Stability of a numerical scheme refers to its ability to converge to the exact solution. A scheme is said to be stable when there happens to be an upper and lower bound on the errors. Otherwise, with unbound errors, the solution will "blow up" and the numerical approximation will be nowhere close to the exact solution.

2.2.1 Convection Discretization

Fluid flow problems are represented by differential equations which can be a convection or a convection-diffusion equation. To evaluate these equations numerically, the first step is to discretize the convection terms. This section deals with the discretization schemes for convection terms using the finite difference method.
The finite difference method is believed to be the oldest method used for numerical solution of partial differential equations, introduced by Euler in the 18th century[11]. It is a simple method which uses the direct definition of derivatives to discretize the equation. Taylor expansion is used to determine the truncation error and the order of approximation. This method works very well with a Cartesian grid system as the calculation of derivatives will be, simply, the difference of values across two points, divided by the grid size.
The points used for the approximation in a scheme can be represented in geometric sketch called the stencil. A stencil gives an idea of the order of the scheme, number of points used in the scheme and the nature of the scheme− implicit or explicit. A wider stencil signifies a higher order of accuracy. A stencil with more than one point at the new time step, $n+1$, signifies that the scheme is implicit. In an implicit scheme, equation for calculating an unknown variable at a new time step has the unknown variable on both sides of the equation. On the other hand, explicit schemes, as the name implies, have an explicit definition for an unknown variable.
Following are a few schemes which can be employed for convection discretization:

- First Order Upwind (FOU) Scheme
  The FOU scheme is, as the name suggests, a first order scheme which uses

the values of the cells upstream from the position where the variable is to be evaluated. Upwind implies that the terms are evaluated in the direction of the flow. Following is an example of FOU discretization,

$$\frac{\partial U}{\partial x_j} = \frac{(U_i - U_{i-1})}{\Delta x_j}$$

- Central Difference Scheme (CDS)
  This scheme utilizes grid points lying on either side of the point at which the variable is to be evaluated. It is a second order scheme.

  $$\frac{\partial U}{\partial x} = \frac{U_{i+1} - U_{i-1}}{2\Delta x}$$

  CDS schemes are easy to implement compared to higher order upwind schemes as one does not have to check the direction of the flow. But this scheme is unconditionally unstable for damped differential equations. This means for a an equation with a friction term (or in this case viscosity), the scheme would not perform as expected.

- Sharp and Monotonic Algorithm for Realistic Transport (SMART) Scheme
  This scheme was introduced in 1988 as a new approach to approximating the convection terms in a steady state transport equation[12]. A technique called 'curvature compensation' was used to develop a polynomial based discretization scheme. This scheme is up to second order accurate. The main advantage of this method is that it is a second order scheme and this provides for numerical stability. This makes it attractive to use to solve a 3-dimensional fluid flow problem.

- Weighted Essentially Non- Oscillatory (WENO) Scheme
  Essentially Non-oscillatory (ENO) scheme is an adaptive stencil scheme developed by Harten and Osher in 1987. In this scheme, each cell has its own stencil of cells. Then, by selecting the stencil which gives the smoothest solution, spurious oscillations are avoided. Liu et al. [20], in 1994, went ahead to modify this scheme such that instead of selecting just one "smoothest" stencil, multiple stencils are chosen and assigned weights on the basis of the smoothness of the solutions. A convex combinations of the candidate stencils then leads to a solution with a non oscillatory property in this scheme. The main advantage of this scheme is, that unlike other higher order schemes like the MUSCL[33] or the TVD[14], the local extrema are preserved. In the regions where the solutions are smooth, this scheme is accurate to the 5^{th} order and in presence of large gradients, it reduces to a minimum of 3^{rd} order. This study employs the WENO

scheme for convection discretization with the Hamilton-Jacobi formulation[17]. An example of implementation of this scheme to the level set function, ϕ is presented below.
Depending on the velocity at a location, the level set function can be defined to be:

$$\phi_x = \begin{cases} \phi_x^- & if\ U_1 > 0 \\ \phi_x^+ & if\ U_1 < 0 \\ 0 & if\ U_1 = 0 \end{cases} \tag{2.5}$$

The WENO approximation for $\phi_x^{\pm}$ is a convex combination of the three possible ENO approximations:

$$\phi_x^{\pm} = \omega_1^{\pm}\phi_x^{1\pm} + \omega_2^{\pm}\phi_x^{2\pm} + \omega_3^{\pm}\phi_x^{3\pm} \tag{2.6}$$

The three ENO stencils defined for ϕ are

$$\begin{aligned} \phi_x^{1\pm} &= \frac{q_1^{\pm}}{3} - \frac{7q_2^{\pm}}{6} + \frac{11q_3^{\pm}}{6} \\ \phi_x^{2\pm} &= -\frac{q_2^{\pm}}{6} + \frac{5q_3^{\pm}}{6} + \frac{q_4^{\pm}}{3} \\ \phi_x^{3\pm} &= \frac{q_3^{\pm}}{3} + \frac{5q_4^{\pm}}{6} - \frac{q_5^{\pm}}{6} \end{aligned} \tag{2.7}$$

with,

$$\begin{aligned} q_1^- &= \frac{\phi_{i-2} - \phi_{i-3}}{\Delta x},\ q_2^- = \frac{\phi_{i-1} - \phi_{i-2}}{\Delta x},\ q_3^- = \frac{\phi_i - \phi_{i-1}}{\Delta x}, \\ q_4^- &= \frac{\phi_{i+1} - \phi_i}{\Delta x},\ q_5^- = \frac{\phi_{i+2} - \phi_{i+1}}{\Delta x} \end{aligned} \tag{2.8}$$

and

$$\begin{aligned} q_1^+ &= \frac{\phi_{i+3} - \phi_{i+2}}{\Delta x},\ q_2^+ = \frac{\phi_{i+2} - \phi_{i+1}}{\Delta x},\ q_3^+ = \frac{\phi_{i+1} - \phi_i}{\Delta x}, \\ q_4^+ &= \frac{\phi_i - \phi_{i-1}}{\Delta x},\ q_5^+ = \frac{\phi_{i-1} - \phi_{i-2}}{\Delta x} \end{aligned} \tag{2.9}$$

the weights are written as:

$$\omega_1^{\pm} = \frac{\alpha_1^{\pm}}{\alpha_1^{\pm} + \alpha_2^{\pm} + \alpha_3^{\pm}},\ \ \omega_2^{\pm} = \frac{\alpha_2^{\pm}}{\alpha_1^{\pm} + \alpha_2^{\pm} + \alpha_3^{\pm}},\ \ \omega_3^{\pm} = \frac{\alpha_3^{\pm}}{\alpha_1^{\pm} + \alpha_2^{\pm} + \alpha_3^{\pm}}, \tag{2.10}$$

and

$$\alpha_1^{\pm} = \frac{1}{10}\frac{1}{\left(\widetilde{\epsilon} + IS_1^{\pm}\right)^2}, \quad \alpha_2^{\pm} = \frac{6}{10}\frac{1}{\left(\widetilde{\epsilon} + IS_2^{\pm}\right)^2}, \quad \alpha_3^{\pm} = \frac{3}{10}\frac{1}{\left(\widetilde{\epsilon} + IS_3^{\pm}\right)^2} \tag{2.11}$$

with the regularization parameter $\widetilde{\epsilon} = 10^{-6}$ in order to avoid division by zero and the following smoothness indicators:

$$\begin{aligned} IS_1^{\pm} &= \frac{13}{12}\left(q_1 - 2q_2 + q_3\right)^2 + \frac{1}{4}\left(q_1 - 4q_2 + 3q_3\right)^2, \\ IS_2^{\pm} &= \frac{13}{12}\left(q_2 - 2q_3 + q_4\right)^2 + \frac{1}{4}\left(q_2 - q_4\right)^2, \\ IS_3^{\pm} &= \frac{13}{12}\left(q_3 - 2q_4 + q_5\right)^2 + \frac{1}{4}\left(3q_3 - 4q_4 + q_5\right)^2 \end{aligned} \tag{2.12}$$

2.2.2 Time Discretization

In cases of fluid dynamics where the flow characteristics change rapidly over time, it is essential to have a highly accurate discretization scheme for the time dependent terms. REEF3D has the Adam-Bashforth and third and fourth order TVD Runge-Kutta schemes included in the code for this purpose. These are explicit methods which are easy to construct and apply, even for higher orders.

- Adam-Bashforth Scheme
  This scheme is second order accurate, which utilizes values from two previous time steps to compute the value at the next time step. An example of application of this scheme to the level set function is presented below:

$$\phi^{n+1} = \phi^n + \frac{\Delta t_n}{2}\left(\frac{\Delta t_n + 2\Delta t_{n-1}}{\Delta t_{n-1}} L\left(\phi^n\right) - \frac{\Delta t_n}{\Delta t_{n-1}} L\left(\phi^n\right)\right) \tag{2.13}$$

- Total Variance Diminishing (TVD) 3^{rd} order Runge-Kutta Scheme
  A TVD scheme, developed by Harten [14], is an explicit numerical scheme that preserves the monotonicity of the solution. It implies that there are no wiggles in the solution as the local extrema are suppressed to maintain monotonicity. An example of the TVD scheme is the TVD Runge-Kutta scheme [28]. An example of application of the third order TVD Runge-Kutta scheme is as follows

$$\begin{aligned} \phi^{(1)} &= \phi^n + \Delta t L\left(\phi^n\right) \\ \phi^{(2)} &= \frac{3}{4}\phi^n + \frac{1}{4}\phi^{(1)} + \frac{1}{4}\Delta t L\left(\phi^{(1)}\right) \\ \phi^{n+1} &= \frac{1}{3}\phi^n + \frac{2}{3}\phi^{(2)} + \frac{2}{3}\Delta t L\left(\phi^{(2)}\right) \end{aligned} \tag{2.14}$$

This being a three step scheme, the spatial derivatives have to be calculated three times. So, this scheme is computationally more demanding than the Adam-Bashforth scheme.

- 4^{th} order Runge-Kutta Scheme A discretization scheme of a higher order under is the 4^{th}-order Runge-Kutta scheme. This scheme is a four step scheme and provides higher accuracy in the simulations. It is computationally more demanding than the previous two discussed above. The solutions are expected to be more accurate due to the higher order of this scheme. An example of its implementation is shown below:

$$\begin{aligned}
\phi^{(1)} &= \phi^n + \frac{\Delta t}{2} L\left(\phi^n\right) \\
\phi^{(2)} &= \phi^n + \frac{\Delta t}{2} L\left(\phi^{(1)}\right) \\
\phi^{(3)} &= \phi^n + \Delta t L\left(\phi^{(2)}\right) \\
\phi^{n+1} &= \frac{-1}{3}\phi^n + \frac{1}{3}\phi^{(1)} + \frac{2}{3}\phi^{(2)} + \frac{1}{3}\phi^{(3)} + \frac{\Delta t}{6} L\left(\phi^{(3)}\right)
\end{aligned} \tag{2.15}$$

2.2.3 Adaptive Time Stepping

To obtain a good numerical solution, it is essential that the fluid being simulated does not move a distance that is more than the computational grid size in one time step. This statement is the simplified content of a condition called the Courant condition[7]. Mathematically, it can be summarized as:

$$\frac{u\Delta t}{\Delta x} \leq C \tag{2.16}$$

This condition called the Courant condition is implemented in implicit time stepping algorithms. The current study utilizes explicit time stepping methods, described in section 2.2.2. To maintain an adequate time step size using explicit methods, a condition called the CFL criterion is applied, where the time step size for the next step is guided by the maximum values of velocities, viscosity and the volume and surface forces in the current time step, following the CFL condition proposed by Courant, Friedrichs and Lewy:

$$\delta t \leq 2\left(\left(\frac{|u|_{max}}{\delta x} + V\right) + \sqrt{\left(\frac{|u|_{max}}{\delta x} + V\right)^2 + \frac{4\,|S_{max}|}{\delta x}}\right)^{-1} \tag{2.17}$$

with

$$V = max\left(\nu + \nu_t\right) \cdot \left(\frac{2}{\left(\delta x\right)^2} + \frac{2}{\left(\delta y\right)^2} + \frac{2}{\left(\delta z\right)^2}\right) \tag{2.18}$$

2.3 Solution of the Navier Stokes Equation

Before proceeding to solve the fluid flow problem, it is important to make a note of the features of the Navier Stokes equations presented in equation (2.4) (reproduced below) and the challenges posed by it in arriving at a solution. This aids in charting a procedure to deal with the fluid flow problem.

$$\frac{\partial U_i}{\partial t} + U_j \frac{\partial U_i}{\partial x_j} = -\frac{1}{\rho}\frac{\partial P}{\partial x_i} + \frac{\partial}{\partial x_j}\left[\nu\left(\frac{\partial U_i}{\partial x_j} + \frac{\partial U_j}{\partial x_i}\right)\right] + g_i$$

The first aspect that is to be noted here is that the pressure is included as source term. But, there is no definition for the advection of the pressure. It is also to be noted that the advection in the equation is non-linear. As mentioned in section 2.1, the Navier Stokes equations are produced by coupling the mass and momentum equations. Hence, the result is that velocity terms are coupled in to a non-linear term in the Navier Stokes equations.

The above aspects pose the following challenges to the solution of the Navier Stokes equations. Due to the absence of a definition for evolution of pressure, a direct approach to determining the pressure at the next grid point is not available. The presence of non-linear terms also pose a challenge to arriving at an analytical solution because it would involves use of implicit methods which can be lengthy and computationally expensive. An alternative would be to explore suitable iterative methods.

One of the methods to solve for equation (2.4) is the projection method proposed by Chorin [5]. In this method, an intermediate velocity field is first obtained by ignoring the pressure gradient. The intermediate velocity U_i^* is computed using the transient equation:

$$\frac{\partial(U^* - U_i^n)}{\partial t} + U_j^n \frac{\partial U_i^n}{\partial x_j} = \frac{\partial}{\partial x_j}\left[\nu(\phi^n)\left(\frac{\partial U_i^n}{\partial x_j} + \frac{\partial U_j^n}{\partial x_i}\right)\right] + g_i \tag{2.19}$$

At this stage, the intermediate velocity field U_i^* may be erroneous and may not satisfy the continuity equation. In the second step, the projection step, pressure is used to determine the velocity at the next time step, $n+1$.

$$\frac{\partial(U_i^{n+1} - U_i^*)}{\partial t} + \frac{1}{\rho(\phi^n)}\frac{\partial P^{n+1}}{\partial x_i} = 0 \tag{2.20}$$

To solve the above equation 2.20, the value of the pressure term, P^{n+1} needs to be known. This is obtained by using the divergence operator on equation (2.20). A condition that the divergence of U_i^{n+1} is zero is applied. This condition arises from the continuity equation, which provides for a divergence free velocity field. The equation obtained then is called the Poisson pressure equation, formulated as:

$$\frac{\partial}{\partial x_i}\left(\frac{1}{\rho(\phi^n)}\frac{\partial P}{\partial x_i}\right) = -\frac{1}{\Delta t}\frac{\partial U_i^*}{\partial x_i} \tag{2.21}$$

The value of pressure obtained from this step is then used in the equation 2.20 and the velocity at the new time step is determined, which complies with the continuity equation. This occurs due to the condition of zero divergence applied to the velocity field to arrive at equation 2.21. Upon solving this equation, the Navier Stokes equations are solved. The method to obtain a solution for equation 2.21 is presented in the following section.

2.3.1 Pressure Solver

To solve eqn. (2.21), direct methods such as the Gaussian elimination are too expensive in terms of computational resources. Thus, an iterative method is employed here. The various iterative methods that can be employed are: Jacobi method, Gauss-Siedel method, Successive Over-Relaxation method, Conjugate Gradient method, Bi-Conjugate Gradient method and Multigrid method.
There are two classes of iterative solvers for non-linear equations: Newton-like solvers and Global solvers. Newton-like methods solve an equation by linearizing it about an an initial estimated value of the solution using the first two terms of the Taylor series. These methods converge very quickly if the initial estimate of the result is close to the final solution. A bad initial estimate will impede the convergence.
Global solvers arrive at a solution by converting the equation to a minimization problem. This means the solver tries to find the minimum of a function. This is done by searching for the lowest point on the surface, which lies in the opposite direction of the gradient of the function. This process of finding the minimum on a line on the surface defined by the function is carried out iteratively until it converges to the solution. This method is guaranteed to converge irrespective of the initial value, but the rate of convergence is found to be very slow. Also, in functions which have minor undulations, the solver would oscillate back and forth between two successive minima. This happens because the solver searches for the minima in only one direction. In order to effectively use this approach, it is required to have a solver which can minimize the function more efficiently.
The Conjugate Gradient (CG) method, developed by Hestenes and Stiefel in 1952 is

an example of an improved global solver. The distinguishing feature of the CG solver is that it is able to minimize a function in several directions while searching in one direction. The name 'conjugate' is derived from the fact that the principle is valid when the two directions are conjugate, that is, the vectors are orthogonal. This can be extended to as many directions as needed.
The CG method, though, is limited in its application to symmetric systems only. Generally, problems in fluid dynamics deal with non-symmetric equations like the convection-diffusion equations. Hence, the CG method cannot be employed in these cases. The Bi-Conjugate Gradient (BiCG) method, developed by Fletcher in 1976, gets around this problem by first converting the non-symmetric system into a symmetric system, by the use of a transpose matrix. This process results in the BiCG method requiring twice the computational effort compared to the CG method, but converges at about the same rate[11].
The Bi-Conjugate Gradient Stabilized (BiCGSTAB) method, is an improvement over the BiCG, which converges faster and produces more accurate solutions[32]. A preconditioned BiCGSTAB is used in this study to solve the for pressure. Preconditioning means replacing the problem to be solved by another problem with the same solution, but which is known to converge faster.

2.4 Turbulence Modelling

The interaction of fluids with a structure can give rise to turbulence in the flow. One of the effects of turbulence is the production of vortices in the flow field downstream of the structure. This change in the flow pattern has an effect on the force experienced by the structure. Thus, a turbulence model has to be incorporated in the code to account for phenomena arising due to turbulence. Turbulence modelling is carried out in this study using the Wilcox's k-ω model[34] together with the Reynolds Averaged Navier Stokes (RANS) equation. This concept is employed in the study during the phase of force calculation (Chapter 4). The validation and testing phase of the wave tank Chapter 3 uses the Navier Stokes equation and two dimensional simulations since there is is no turbulent phenomena to be dealt with.
The k-ω model is a two-equation model, which uses two additional transport equations to account for turbulence in the computational domain. One of the variables transported is the turbulent kinetic energy, k, which determines the energy in the turbulence. The other variable is the specific turbulent dissipation, ω, which is used to determine the scale of turbulence in the simulation. Due to the fact that both the energy and scale of turbulence are calculated, this model can be used in any scenario with turbulence, without prior knowledge of the scale of the turbulence. The eddy viscosity, ν_t, is then determined using these variables.

The RANS equation is obtained by including the Reynolds stress terms to the Navier Stokes equations (equation 2.4) as shown below:

$$\frac{\partial U_i}{\partial t} + U_j \frac{\partial U_i}{\partial x_j} = -\frac{1}{\rho}\frac{\partial P}{\partial x_i} + \frac{\partial}{\partial x_j}\left[\nu\left(\frac{\partial U_i}{\partial x_j} + \frac{\partial U_j}{\partial x_i}\right) - \overline{u_i u_j}\right] + g_i \tag{2.22}$$

The stress terms added to the Navier Stokes equations, $\overline{u_i u_j}$, represent the momentum fluxes arising from the coupling of the Navier Stokes equations with the continuity equation. This introduces non-linearity in the equation and extra unknown quantities. The closure of the equations now becomes a challenge due to the presence of more unknown variables than equations. To solve the RANS equation, the stress terms are replaced with the Boussinesq approximation which relates them to the mean strain of the flow:

$$-\overline{u_i u_j} = \nu_t\left(\frac{\partial U_j}{\partial x_i} + \frac{\partial U_i}{\partial x_j}\right) - \frac{2}{3}k\delta_{ij} \tag{2.23}$$

with

$$\nu_t = c_\mu \frac{k}{\omega} \tag{2.24}$$

The transport equations for k and ω are defined as follows:

$$\frac{\partial k}{\partial t} + U_j \frac{\partial k}{\partial x_j} = \frac{\partial}{\partial x_j}\left[\left(\nu + \frac{\nu_t}{\sigma_k}\right)\frac{\partial k}{\partial x_j}\right] + 2\nu_t |S|^2 - k\omega \tag{2.25}$$

$$\frac{\partial \omega}{\partial t} + U_j \frac{\partial \omega}{\partial x_j} = \frac{\partial}{\partial x_j}\left[\left(\nu + \frac{\nu_t}{\sigma_\omega}\right)\frac{\partial \omega}{\partial x_j}\right] + 2c_\mu c_{\omega 1} |S|^2 - c_{\omega 2}\omega^2 \tag{2.26}$$

The values of the closure coefficients used in the equations above are: $c_\mu = 0.09$, $c_{\omega 1} = 5/9$, $c_{\omega 2} = 5/6$ and $\sigma_\omega = \sigma_k = 2$. The term $|S|^2$ is constituted of the mean rate of the strain tensor:

$$S_{ij} = \frac{1}{2}\left(\frac{\partial U_j}{\partial x_i} + \frac{\partial U_i}{\partial x_j}\right) \tag{2.27}$$

At solid boundaries, the surface roughness is accounted for by using Schlichting's rough wall law [27]:

$$U^+ = \frac{1}{\kappa} ln\left(\frac{30d}{k_s}\right) \tag{2.28}$$

where Near the wall, an assumption is made that the turbulent production is equal to the dissipation of k [34]. The wall function for the specific turbulent dissipation ω for a bed cell with the distance Δy_p from the wall to the centre of the cell is then:

$$\omega_{wall} = -\frac{c_\mu^{3/4} k_w^{1/2} U_w^+}{\Delta y_p} \tag{2.29}$$

The formula gives the value for ω directly. The turbulent kinetic energy k at the wall

is treated by integrating the source terms of equation (2.25) over the bed cell:

$$\int (P_k - \epsilon_{wall})\,\rho = \left[\frac{\tau_w U_w}{\Delta y_p} - \frac{\rho c_\mu^{3/4} k_w^{3/2} U_w^+}{\Delta y_p}\right] \tag{2.30}$$

The rough wall law is then used to determine the wall shear stress τ_w and the dimensionless U_w^+. The terms from equation (2.30) are discretized as source terms in the transport equation for k.

2.5 Modelling the Free Surface

In fluid dynamics, it is common to deal with multi-phase flows where the interaction between the interface of the different phases assumes importance due the effect it has on the engineering design. In the field of marine civil engineering, dealing with ocean waves, the free surface of the water is modelled by assuming a two phase flow with air and water. The various methods that can be used for this purpose are Marker and Cell (MAC) approach, Volume of Fluids (VoF) method and the Level Set Method, to name a few. In the MAC method many marker cells are identified on the fluid interface and their convection is calculated in addition to solving the fluid flow problem. This method becomes computationally expensive especially in 3-dimensional simulations, when the number of particles to be calculated becomes very large[11].
The VoF method calculates the free surface by solving an equation for the filled fraction of the control volumes of the fluids involved in the problem. This method is reported to be more efficient than the MAC scheme and also found to work well with problems involving breaking waves. This method is very robust and widely implemented in commercial codes like Ansys Fluent, StarCCM+ and open source CFD code− OpenFOAM. The disadvantage in this method is that the free surface tends to get smeared over two to three cells and needs a local grid refinement to accurately represent the free surface[11].

2.5.1 Level Set Method

The Level Set Method (LSM) is the employed in REEF3D to model the free surface. It uses a signed distance function, called the level set function, which captures the free surface. The property of the level set function, $\phi(\vec{x}, t)$ is such that $\phi(\vec{x}, t) = 0$ at the interface. Away from the interface its value is the closest distance of the point from the interface and the sign of the function denotes the fluid which governs the

point, as illustrated in figure 2.1. Thus, the function is defined as

$$\phi(\vec{x},t)\begin{cases} > 0 & if\ \vec{x}\ is\ in\ phase\ 1 \\ = 0 & if\ \vec{x}\ is\ at\ the\ interface \\ < 0 & if\ \vec{x}\ is\ in\ phase\ 2 \end{cases} \tag{2.31}$$

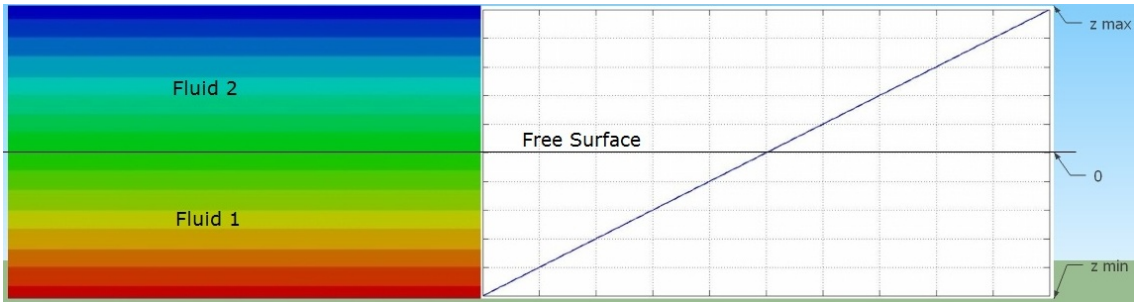

Figure 2.1: The Level Set Function

The movement of the interface is characterized by the convection of the level set function determined by

$$\frac{\partial \phi}{\partial t} + \vec{u}\nabla\phi = 0 \tag{2.32}$$

For immiscible, incompressible fluids the material derivative of density and viscosity, $\frac{D\rho}{Dt}$ and $\frac{D\nu}{Dt}$ is zero. These equations, in the same form as equation (2.32), when discretized directly, lead to numerical instability due to a jump in their values at the interface. The solution to this problem is to define a transition zone with thickness 2ϵ, where ϵ is proportional to the grid spacing and smoothen the region at the interface using a regularized Heavyside function H(ϕ) such that

$$\begin{aligned} \rho(\phi) &= \rho_1 H(\phi) + \rho_2(1 - H(\phi)) \\ \nu(\phi) &= \nu_1 H(\phi) + \nu_2(1 - H(\phi)) \end{aligned} \tag{2.33}$$

where,

$$H(\phi) = \begin{cases} 0 & if\ \phi < -\epsilon \\ \frac{1}{2}\left(1 + \frac{\phi}{\epsilon} + \frac{1}{\pi} sin\left(\frac{\pi\phi}{\epsilon}\right)\right) & if\ |\phi| \leq \epsilon \\ 1 & if\ \phi > \epsilon \end{cases} \tag{2.34}$$

It is notable that, in equation (2.31), the level set function is smooth across the interface. This property makes the function differentiable at the interface and avoids the instability that would occur if the function resembled a step function, that is, with a jump at the interface. This is the main advantage of using the level set method to calculate the interface between the fluids.

2.5.2 Reinitialization

The challenge in using LSM method springs from the fact that the signed distance property of the level set function is not maintained when the interface moves. It means that the value of ϕ does not remain the shortest distance of the point from the interface. To overcome this problem, the function is reinitialized or reset after a certain amount of time, say after every iteration. During this process, the function should be reset without changing the position of the interface.
There are two methods to approach reinitialization, the partial differential equation (PDE) approach and the Fast Marching Method (FMM). This study uses a PDE based reinitialization procedure presented in [30].

$$\frac{\partial \phi}{\partial \tau} + S(\phi)\left(\left|\frac{\partial \phi}{\partial x_j}\right| - 1\right) = 0 \tag{2.35}$$

where S(ϕ) is the smooth signed function by [24]

$$S(\phi) = \frac{\phi}{\sqrt{\phi^2 + \left|\frac{\partial \phi}{\partial x_j}\right|^2 (\Delta x)^2}} \tag{2.36}$$

The signed distance property is then restored by solving equation (2.35) until steady state. The sign function in equation (2.36) assigns the value of zero to the interface. The values for rest of the domain are assigned according to equation (2.31).

2.6 Immersed Boundary - Ghost Cell Method

The numerical methods used in REEF3D are all finite difference methods and they mesh perfectly with the adaptation of a regular grid like the Cartesian grid. This provides for an uncomplicated numerical implementation. On the other hand, a Cartesian grid is not very flexible due to its well defined, regular structure. It can not be 'wrapped' around a complex geometry. This is a problem when one has to deal with irregular structures placed in a fluid domain or an irregular boundary like in a natural channel. One of the solutions to overcome this problem is the Immersed Boundary Method (IBM). This method was initially proposed in 1972[25] for numerical analysis of blood flow in the heart, where the boundaries are elastic. The IBM is incorporated in the Navier Stokes equations as a source term which behaves like an elastic spring. To apply this method to solid boundaries, the stiffness of the spring is set very high. In this way, a boundary is simulated without making any changes to the computational grid.
Further advances on the IBM method led to the formulation of the Ghost Cell IBM

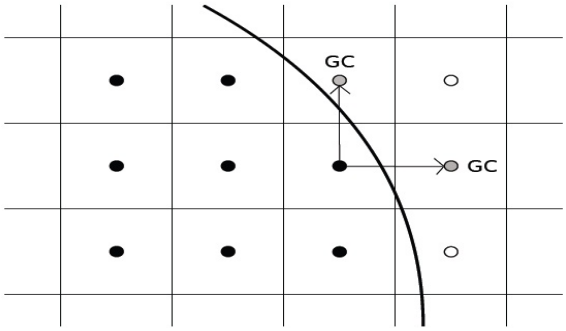

Figure 2.2: Ghost Cell Immersed Boundary

(GCIBM)[31]. In this method, the values from the fluid region are extrapolated into the solid region and these cells are called 'ghost cells'. The ghost cell value is computed along an orthogonal line across the boundary as illustrated in figure 2.2. An improvement to the GCIBM method was to extend the solution smoothly across the boundary in the same direction as the discretization for which it would be used[3]. But, there could be scenarios where the ghost cells are updated from multiple directions. So, it is prudent to adapt the ghost cells to store multiple values and return the respective values when called from a particular direction. This concept is called the Multiple Ghost Cell (MGC), which has been created for and utilized in REEF3D[4] and realized through object oriented programming techniques.

2.7 Parallel Processing

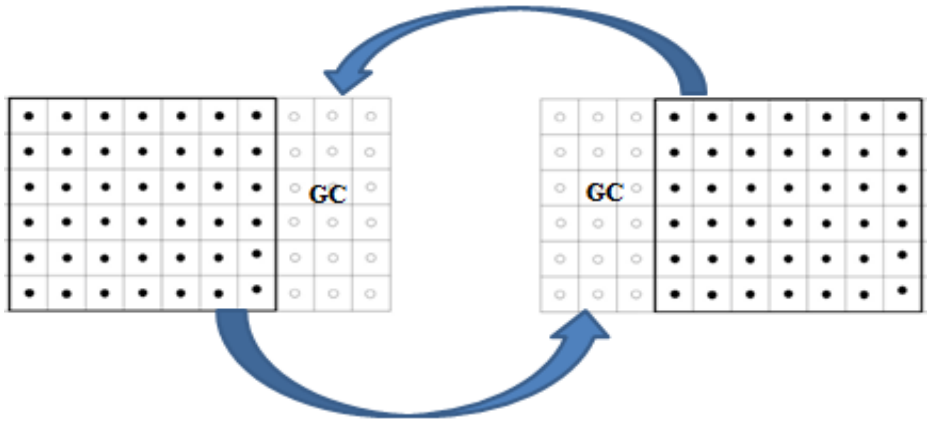

Figure 2.3: Working of MPI - Exchange of values

With the advent of multi-core computers, which have multiple processing elements on a single computer, it is possible to improve the performance of a code by adapt-

ing it to parallel processing. Parallel processing refers to dividing a large problem into smaller parts and solving them simultaneously. REEF3D has been adapted for parallel processing by the use of a method called Message Passing Interface (MPI). The computational domain is explicitly split into smaller pieces and assigned to different processors. The values at the boundaries of each process have to be then shared among the neighbouring processes for the simulation to continue. To enable this sharing, the values of the cells at either edge of an individual process are copied and transmitted to the respective boundaries of the previous and next processes and stored on a set of ghost cells at the process boundary. This process of information exchange is handled by the Application Programming Interface (API). An illustration is presented in figure 2.3 MPI is structured such that it can be used on both shared memory and distributed memory architectures.

Chapter 3

Numerical Wave Tank

Studies in the field of marine and offshore engineering using CFD need a way to simulate an environment with wave generation and absorption to calculate the hydrodynamics around marine structures. This is enabled by a numerical wave tank. The numerical experiments carried out here have to mimic the physical experiments carried out in a wave flume in the laboratory. Numerical wave tanks can be based on different approaches to carry out their solutions. Two popular approaches are the RANS approach and the potential theory approach. Further, the available choices for the numerical treatment of these approaches provides a large number of combinations to be studied to arrive at a good combination for a certain engineering scenario. Some of the combinations are

- Potential theory with finite element discretization
- RANS equations with free surface description by VoF method
- RANS equations with free surface description by LSM
- Combination of potential theory and RANS equations

A study[6] has reported the results obtained using the first two approaches listed above. This study uses the RANS equations with free surface obtained using LSM. The last item, a combination of methods, could be a subject of future inquiry. It has been reported that the use of potential theory with the method of finite elements results in a fast and accurate solution, though, RANS equations are preferred for the simulation of wave-structure interactions[6].
In the implementation of the potential theory for numerical modelling of waves, a

Fully Non-linear Potential Flow (FNPF) model has been proposed[13]. In this model, Green's identity is used to transform the Laplace equations for velocity potential (Φ) and its time derivative ($\frac{\partial \Phi}{\partial t}$) to obtain two Boundary Integral Equations (BIE). The solution to these BIEs is obtained using a method called the Boundary Element Method (BEM). Unlike the current study, which uses domain discretization (and method of finite differences), the FNPF model describes the domain through shape functions or splines and the boundary is divided into a finite number of elements. In the process of the solution, the BIEs yield a finite number of linear algebraic equations. The system of equations is then solved and the values of the unknowns is then determined. After this solution, the unknowns inside the domain can be calculated explicitly without the need for numerical approximation. This is the distinct difference between the domain discretization methods and BEM.
Open source CFD software OpenFOAM was also used in a study to develop a numerical wave tank[1]. Here, space discretization was carried out by finite volume approach and the free surface was determined by VoF method. The study concluded that about 200 to 400 grids per wavelength were required to obtain acceptable results.
In a further development, a wave generation toolbox was also developed for OpenFOAM with a new method for wave generation and absorption in the wave tank[16].

3.1 Wave Generation and Absorption

One of the early works in numerical wave generation by a wavemaker in physical space was presented by Kim et al.[18]. This model was limited to non-breaking waves. This model was an application of the Fully Non-linear Potential Flow (FNPF) theory. Two main methods used, so far, for numerical wave generation are

- Moving a wavemaker boundary: In this case, the normal velocities are specified over the surface of a plane paddle. This surface behaves similar to the wavemaker used in the laboratory. Similar to the motion of the physical wavemaker, the numerical surface is moved to generate the waves in the numerical wave tank. The disadvantage in this method is that, it can produce waves that travel opposite to the intended direction, just like the problem faced in a physical model.

- Inclusion of source term: This method generates waves by including a source term in the governing equation, that introduces oscillations in the computational domain. Waves are produced in both directions in this method. The scattered waves are then allowed to travel towards the open boundary and exit the computational domain.

3.1.1 Relaxation Method

This study uses a method attributed to Larsen et al. [19] where the simulated waves are moderated after every time step with an analytical solution. The wave generation region gradually moves from a fully analytical solution to a computational solution. This method of using a combination of analytical and computational values is referred to as the 'relaxation method'. For this purpose, 'relaxation zones' are introduced in the wave tank. The relaxation zones are controlled areas of the numerical wave tank where relaxation functions are applied at various regions in the wave tank to generate the waves at the beginning, absorb the waves at the end and to prevent reflected waves from affecting the wave generation. Three relaxation zones are required to carry out these functions. Each zone has its own relaxation function associated with it. A typical scenario, showing the division of the wave tank into functional zones

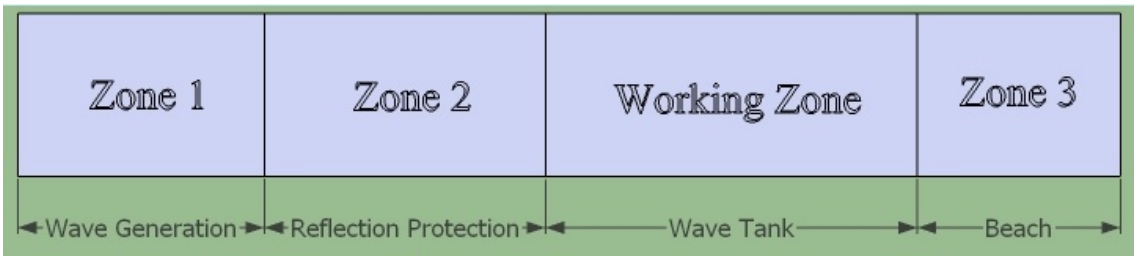

Figure 3.1: Sections of a Numerical Wave Tank

is illustrated in figure 3.1. The first zone, zone 1, takes care of wave generation. The second zone, right after zone 1, prevents reflected waves from affecting the wave generation. The third zone is the numerical beach, which absorbs the waves at the end of the tank. In the absence of zone 3, waves are reflected from the domain boundary and this scenario can be used to simulate the formation of standing waves. The relaxation in zone 1 and 2 is achieved using the following rules on pressure and velocity in the zones:

$$\begin{aligned} U_{relaxed} &= \Psi(x)U_{analytical} + (1 - \Psi(x))U_{computational} \\ P_{relaxed} &= \Psi(x)P_{analytical} + (1 - \Psi(x))P_{computational} \end{aligned} \tag{3.1}$$

Similarly, the relaxation in zone 3 is achieved by the following set of rules for pressure and velocity:

$$\begin{aligned} U_{relaxed} &= \Psi(x)U_{computational} + (1 - \Psi(x))U_{analytical} \\ P_{relaxed} &= \Psi(x)P_{computational} + (1 - \Psi(x))P_{analytical} \end{aligned} \tag{3.2}$$

The function associated with $\Psi(x)$ changes according to the zone on which the relaxation is being applied. The idea behind the application of equation (3.1) is that the

initial computational values of velocity and pressure are gradually transitioned the analytical values, in accordance to the wave theory being applied, at the beginning of the simulation. The computational values are the boundary conditions applied to generate the required wave in the tank.
In the second zone, the analytical values from the end of the first zone are gradually changed to the computational values and the wave enters the working region of the numerical wave tank. This function can be envisioned by considering a reflected wave that is travelling towards the wave generation zone. This reflected wave obviously belongs to the computational values produced in the wave tank. As the wave travels from the working zone of the wave tank, towards the wave generation zone, the computational values are replaced gradually by the analytical values. At the boundary between zone 2 and zone 1, the solution is purely analytical. In this way, the reflected or scattered wave is virtually damped and prevented from affecting wave generation. The relaxation function for zone 3, in equation (3.2), is designed to transition the computational values from the working zone of the wave tank to the analytical values at the beach. The analytical values at the end of the wave tank conform to the fluid velocity coming down to zero as the wave is damped, simulating a beach.

3.1.2 Relaxation Functions

Relaxation functions are functions that are applied over the relaxation zones in order to achieve the required objective of each zone. A set of relaxation functions were proposed by Engsig-Karup[9] for wave absorption and generation respectively as follows

$$\Psi(x) = (1-x)^p \tag{3.3}$$

$$\Psi(x) = -2x^3 + 3x^2 \tag{3.4}$$

Using $(1-x)$ in equation (3.4), produces the function for absorbing reflected waves, so as to not affect the wave generation,

$$\Psi(x) = -2(1-x)^3 + 3(1-x)^2 \tag{3.5}$$

The term p in equation (3.3) determines the steepness of the relaxation function. A value of $p = 6$ has been used in this study. The figure 3.2 illustrates the shapes of the relaxation functions in their respective zones. A rule of thumb suggested in [9] is to extend the relaxation zone over 1-2 times the wavelength of the wave being simulated. Another set of relaxation functions were proposed by Jacobsen et al. [16] for wave generation and absorption.

$$\Gamma_R(\chi_R) = 1 - \frac{exp(\chi_R^{3.5}) - 1}{exp(1) - 1} \; for \; \chi_R \in [0; 1] \tag{3.6}$$

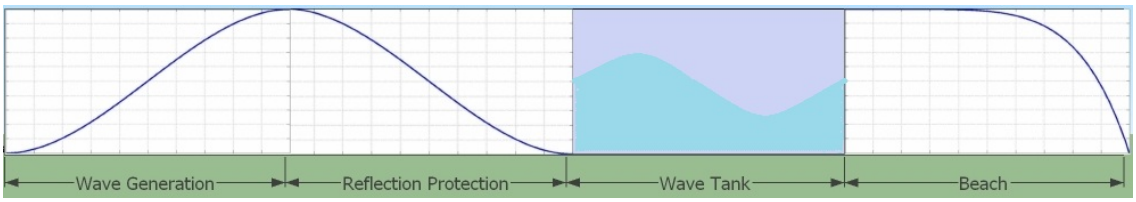

Figure 3.2: Form of Relaxation Functions in the Wave Tank

This form of relaxation proposes to improve the solution by using the values from the cell centres rather than from the cell edges as done in previous works. The motivation behind the development of this method was to avoid the need for a higher resolution grid around the interface. This method was developed for the wave generation toolbox for OpenFOAM which uses the finite volume approach and VoF method for calculating the interface. In this method, the numerical wave tank has only two relaxation zones− at the inlet and the outlet. The intermediate zone, zone 2, is not included in this method. In the current study, it is a matter of interest to observe the behaviour of this method and its suitability for REEF3D, which implements a Cartesian grid and LSM.

3.2 Wave Theory

To understand the forces acting on marine structures, one has to be able to represent the wave field in the region. Waves are undulations on the surface of the water caused by external forces. Various forces− earthquakes, wind, gravitational to name a few; combined with varying field conditions like water depth and bed slope are deciding factors in the form of the wave. Depending on such various factors, the waves formed on the sea surface differ in their characteristic properties - velocity potential, particle velocity induced etc. A highly simplified representation of waves encountered in marine design is accomplished by defining waves using a wave theory.
Wave theories are categorized as 'linear' and 'non-linear' based on the treatment of the boundary conditions listed below:

- Kinematic Boundary Condition
  This defines the motion of the fluid at the free surface, η:

$$\frac{\partial \eta}{\partial t} + U\frac{\partial \eta}{\partial x} = U_k \tag{3.7}$$

  The physical content of equation (3.7) is that a fluid particle at the surface, stays at the surface.

- Dynamic Boundary Condition
  Dynamic boundary condition deals with the force balance at the free surface. It implies that the pressure at the free surface is equal to the atmospheric pressure. Assuming irrotational flow, such that, the partial derivative of Φ in all directions gives the velocity in that particular direction, the dynamic boundary condition is given by:
  $$\frac{P}{\rho} + \frac{\partial \Phi}{\partial t} + \frac{1}{2}(U_i^2 + U_k^2) + g\eta = 0 \tag{3.8}$$

3.2.1 Linear Wave Theory

The linear wave theory is based on the two fundamental equations- the mass and momentum balance equations (2.2) and (2.4), along with linearized kinematic and dynamic boundary conditions[15]. This theory applies when the wave amplitude is small compared to the wavelength and the water depth. This is condition is referred to as the small amplitude approximation.
With this approximation, the kinematic boundary condition is linearized and reduced at mean water level to
$$\frac{\partial \eta(x,t)}{\partial t} = U_k(x,0,t) \tag{3.9}$$
The dynamic boundary condition is simplified to yield the linearized dynamic condition at the mean water level:
$$\frac{\partial \Phi(x,0,t)}{\partial t} + g\eta(x,t) = 0 \tag{3.10}$$
The linear wave theory, thus, defines η,Φ,u,w and the dispersion relation as[2]:
$$\eta = a\ sin(\omega_f t - k_f x) \tag{3.11}$$
$$\Phi = \frac{ag}{\omega}\frac{cosh\ k_f(z+d)}{cosh\ k_f d}cos(\omega_f t - k_f x) \tag{3.12}$$
$$U_i = \frac{\partial \Phi}{\partial x} = \omega a\frac{cosh\ k_f(z+d)}{sinh\ k_f d}sin(\omega t - k_f x) \tag{3.13}$$
$$U_k = \frac{\partial \Phi}{\partial z} = \omega a\frac{sinh\ k_f(z+d)}{sinh\ k_f d}cos(\omega t - k_f x) \tag{3.14}$$
$$\omega_f^2 = gk_f\ tanh\ k_f d \tag{3.15}$$
The limitation imposed by the small amplitude approximation requires the use of other wave theories to define other kinds of wave motion observed in oceanic and coastal waters.

3.2.2 Non-linear Wave Theories

In section 3.2.1, the boundary conditions have been simplified and linearized. Non-linear wave theories or the finite amplitude wave theories, on the other hand, include higher order terms to solve the boundary conditions. These appear in form of an infinite power series which is truncated at the desired higher order term. Also, the equations are solved at the water surface, rather than the mean water level.

Second Order Stokes Wave Theory

The second order Stokes theory developed by Stokes in 1847, is applicable when the ratio H/d is small. So, the theory is applicable in deep waters and some range of intermediate waters. It formulates the wave characteristics in form of a power series of the wave steepness H/λ[8]. The non-dimensional factor used in the power series known as the perturbation factor. Here, η, Φ, U_i and U_k are formulated as:

$$\eta = a\ cos(k_f x - \omega_f t) + \frac{\pi H}{8}\frac{H}{\lambda}\frac{cosh\ k_f d(2 + cosh\ 2k_f d)}{sinh^3\ k_f d} cos\ 2(k_f x - \omega_f t) \tag{3.16}$$

$$\Phi = \frac{ag}{\omega_f}\frac{cosh\ k_f(d+z)}{cosh\ k_f d} sin\ (k_f x - \omega_f t) + \frac{3\pi C H}{16}\frac{H}{\lambda}\frac{cosh\ 2k_f(d+z)}{sinh^4\ k_f d} sin\ 2(k_f x - \omega_f t) \tag{3.17}$$

$$U_i = \frac{\partial \Phi}{\partial x} = \omega_f a \frac{cosh\ k_f(z+d)}{sinh\ k_f d} sin(k_f x - \omega_f t) + \frac{H}{\lambda}\frac{3\pi^2 H\ cosh(2k_f(d+z))}{4T\ sinh^4\ k_f d} cos2(k_f x - \omega_f t) \tag{3.18}$$

$$U_k = \frac{\partial \Phi}{\partial x} = \omega_f a \frac{cosh\ k_f(z+d)}{sinh\ k_f d} sin(k_f x - \omega_f t) + \frac{H}{\lambda}\frac{3\pi^2 H\ sinh(2k_f(d+z))}{4T\ sinh^4\ k_f d} sin2(k_f x - \omega_f t) \tag{3.19}$$

The dispersion relation remains the same as in equation (3.15) for the second order theory. It is to be noticed that the first term in equations (3.16) and (3.17) is the same as the expression for linear wave theory, that is, equations (3.11) and (3.12). The second term in the expressions for η and Φ here are directly dependent on the wave steepness. From these terms the asymmetric nature of the wave is realized, where the troughs are shallower and the crests are higher, than linear waves of the same amplitude. This vertical asymmetry increases with an increase in wave steepness.

Fifth Order Stokes Wave Theory

With an increase in wave height, it becomes essential to evaluate higher order perturbations to obtain a good representation of the wave. Fenton theory[10] for the analytical solution for the fifth order theory is used in this work. Taylor expansion with the perturbation factor, $\epsilon = \frac{\pi H}{\lambda}$, is evaluated till the fifth power. Thus, the

relations for η,Φ,U_i and U_k according to this theory are:

$$\eta = \frac{1}{k_f} \sum_{n=1}^{5} \epsilon^n b_n \; cos(n\theta) \tag{3.20}$$

$$\begin{aligned} where, b_1 &= 1 + \epsilon^2 B_{31} - \epsilon^4 (B_{53} + B_{55}) \\ b_2 &= B_{22} + \epsilon^2 B_{42} \\ b_3 &= -B_{31} + \epsilon^2 B_{53} \\ b_4 &= B_{44} \\ b_5 &= B_{55} \end{aligned} \tag{3.21}$$

$$\Phi = C_0 \sqrt{\frac{g}{k^3}} \sum_{n=1}^{5} \epsilon^n a^n cosh(nkz) sin(n\theta) \tag{3.22}$$

$$\begin{aligned} where, a_1 &= A_{11} + \epsilon^2 A_{31} + \epsilon^4 A_{51} \\ a_2 &= A_{22} + \epsilon^2 A_{42} \\ a_3 &= A_{33} + \epsilon^2 A_{53} \\ a_4 &= A_{44} \\ a_5 &= A_{55} \end{aligned} \tag{3.23}$$

$$U_i = C_0 \sqrt{\frac{g}{k_f}} \sum_{n=1}^{5} \epsilon^n \; n \; a_n cosh(nk_f z) cos(n\theta) \tag{3.24}$$

$$U_k = C_0 \sqrt{\frac{g}{k_f}} \sum_{n=1}^{5} \epsilon^n \; n \; a_n sinh(nk_f z) sin(n\theta) \tag{3.25}$$

The coefficients C_0, A_{ij}, B_{ij} are dimensionless functions of the water depth and wavelength.

3.3 Validation and Testing of the Wave Tank

The first objective of this work is to validate the numerical wave tank. This is done by comparing the numerical results with the results expected from the wave theory. Different parameters are varied to observe their effect on the result. The results obtained in the wave tank after 15 seconds of simulation are used for the analysis to avoid any spurious results which could occur at the beginning of the test.
In the following sections, a 2-dimensional wave tank 15m long and 1m high with 0.5m water depth is used. Parameters like grid cell density, CFL number, numerical beach width, wave amplitude, relaxation method, spatial discretization scheme, time discretization scheme and wave type are varied to test performance of the wave tank

under different configurations. The results of these trials are presented in the following sections.

3.3.1 Effect of grid cell density

The number of grid cells per wavelength is one of the factors that affects the numerical results. A smaller grid size (dx) would imply more number of cells per wavelength and provide better solutions. On the other hand, this higher resolution results in a higher computational time. It is imperative, thus, to arrive at an optimal grid size such that the numerical results are accurate without being too expensive with regard to computation.
In this section, trials are carried out with WENO spatial discretization scheme and 4^{th} order Runge-Kutta time discretization scheme. Fifth order Stokes waves with an amplitude of $0.05m$ are generated in the wave tank and the effect of varying the grid density is observed.
Figure 3.3 presents the solution obtained with 10 grid cells per wavelength. A wave with $\lambda = 1m$ is generated. The grid cell size is set to $0.1m$. A large reduction in wave amplitude as the wave propagates through the wave tank is observed. This happens due to numerical diffusion which occurs due to the low grid density and results in the damping of the amplitude.
In figure 3.4, the solution using 20 grid cells per wavelength is presented. A wave with $\lambda = 2.0m$ is used with a grid size of $0.1m$. An amplitude error is still observed, but less severe than the first trial. Figures 3.5, 3.6 and 3.7 show the solutions obtained for 40, 100 and 200 grid cells per wavelength, obtained using a wave with $\lambda = 2.0m$ and grid size set to $0.05m$, $0.025m$ and $0.01m$ respectively.

It is seen that the numerical solutions start to match the theoretical values at a grid density of 100 grid cells per wavelength. The convergence of the wave amplitude to the expected amplitude on increase of the grid density can be seen in the graph presented in figure 3.8. From this figure it is clear that the numerical diffusion of the wave amplitude ceases considerably at a grid density of 200 cells per wavelength.
A noticeable feature in figure 3.8 is a singular upward bump in the curve for all values of cell density. The amplitude of the wave is increased by about 0.24% at this location for trials with grid density 100 and 200 cells per wavelength. This can be attributed to slight reflection that occurs at the dissipation end of the wave tank. The chance of this being an initialization problem is countered by the fact that the solutions at $t = 20s$ are used in this analysis. This effect is not so significant in tests with grid cell densities less than 40 as the reducing amplitude due to numerical diffusion hides this effect.

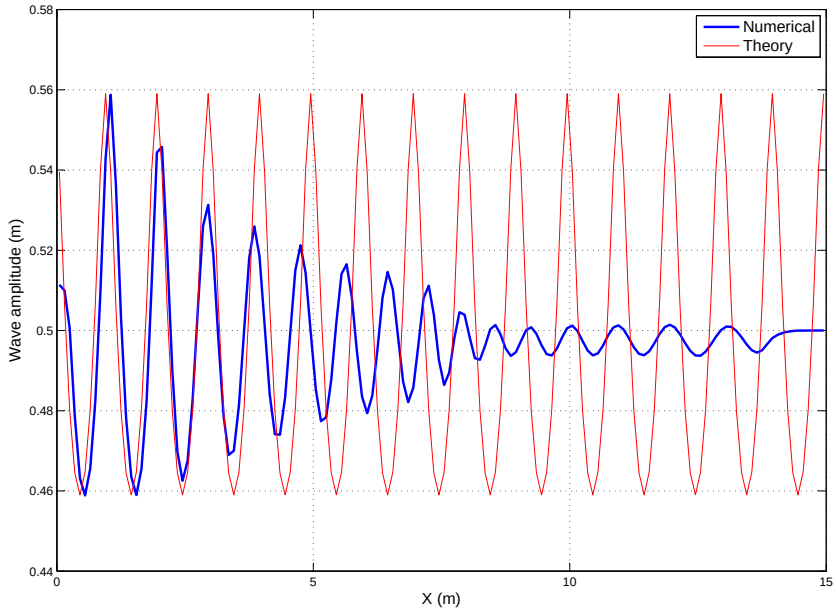

Figure 3.3: Solution with 10 grid cells per wavelength (a=0.05m, λ=1.0m, dx=0.1m)

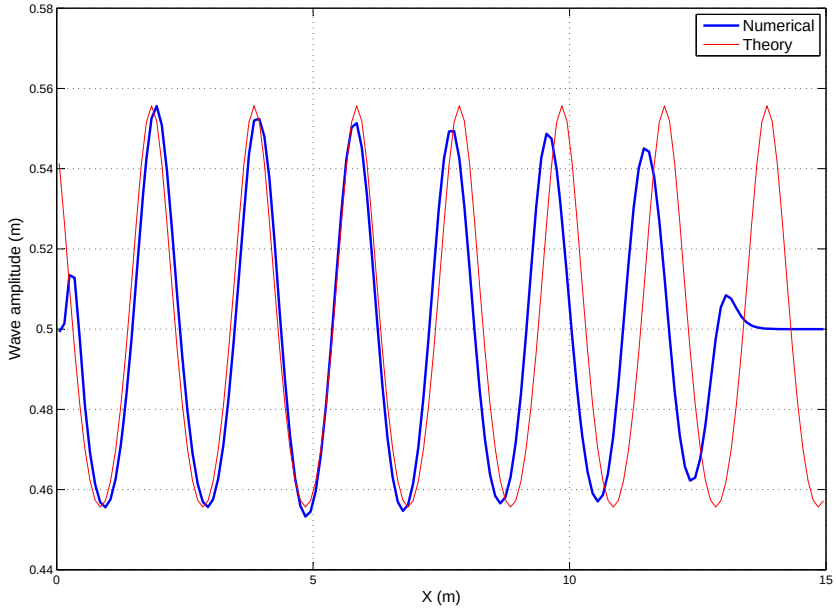

Figure 3.4: Solution with 20 grid cells per wavelength (a=0.05m, λ=2.0m, dx=0.1m)

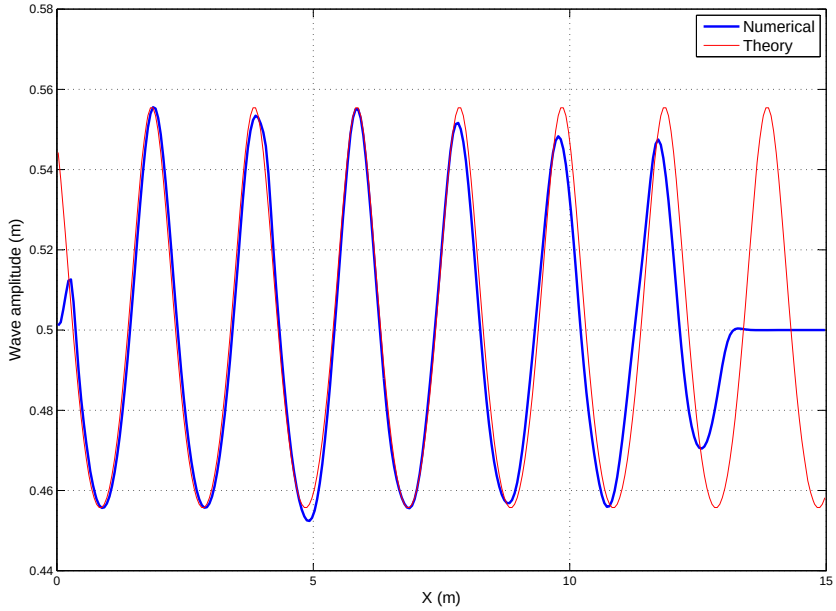

Figure 3.5: Solution with 40 grid cells per wavelength (a=0.05m, λ=2.0m, dx=0.05m)

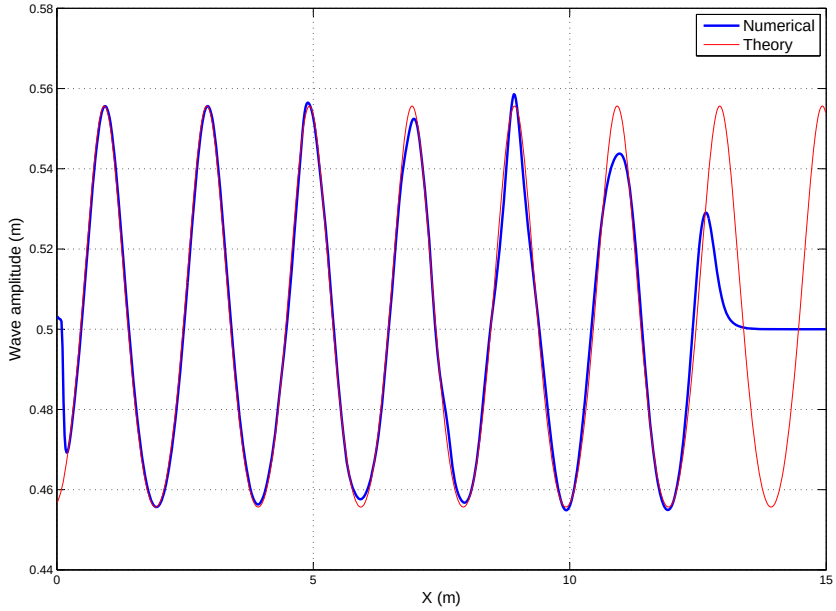

Figure 3.6: Solution with 100 grid cells per wavelength (a=0.05m, λ=2.0m, dx=0.02m)

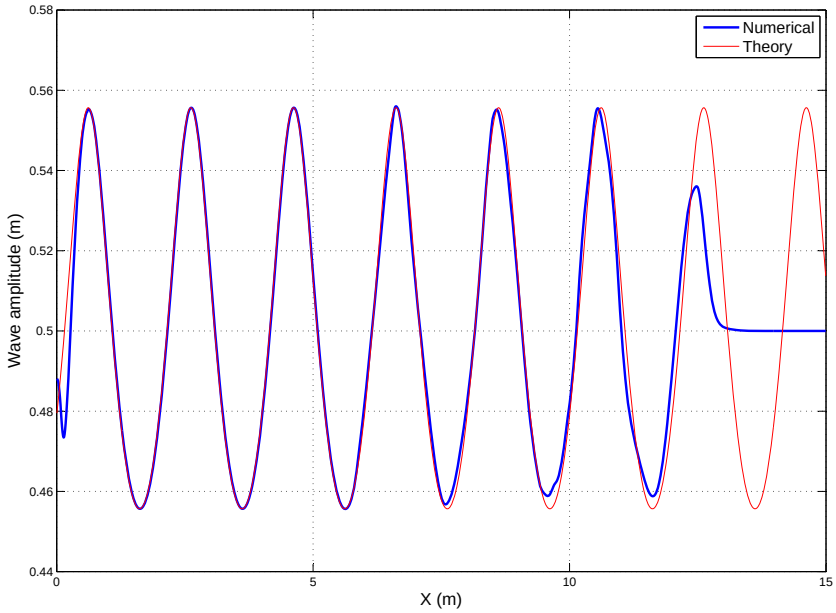

Figure 3.7: Solution with 200 grid cells per wavelength (a=0.05m, λ=2.0m, dx=0.01m)

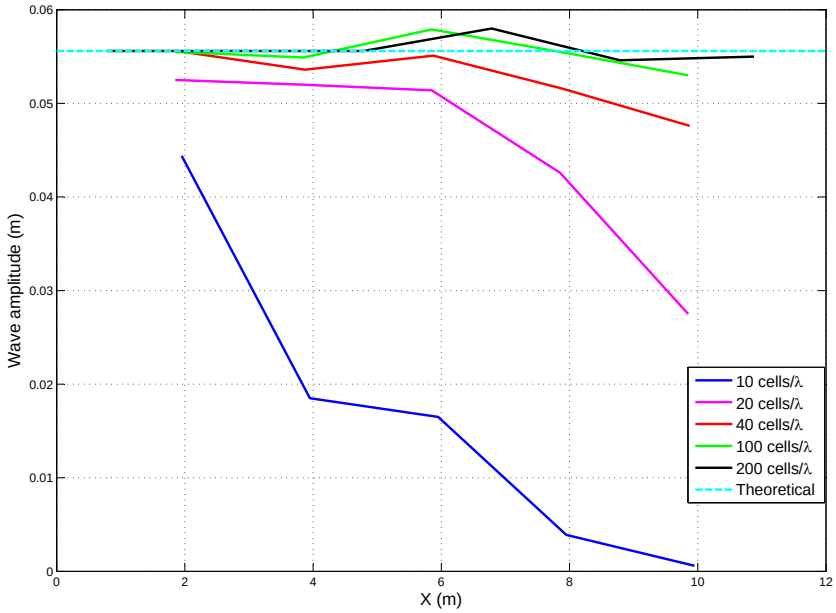

Figure 3.8: Convergence of wave amplitude on increasing grid density

3.3.2 Effect of time step size

The length of the time step is another factor that has to be considered to obtain a good numerical solution. Since adaptive time stepping is employed in this study, the CFL number (section 2.2.3), is used to study the effect of time step size on the solution. Wave amplitude, wavelength and grid size of $0.01m$, $2.0m$ and $0.05m$ respectively and fifth order Stokes waves are used for all the trials in this section.
Figures 3.9 through 3.14 are the solutions obtained by for CFL numbers 0.5, 0.4, 0.3, 0.2, 0.1 and 0.05 respectively. In these figures, it can be observed that not only the wave amplitude is dampened but also the waveform is irregular with multiple peaks in some cases. This effect is reduced with the reduction in the CFL number pointing to the importance of maintaining a suitably low time step to obtain a good solution. The solution with CFL number 0.05 is seen to be almost constant and close to the theoretically expected value. A maximum error of 0.09% is observed in this solution. It has to be mentioned, though, that this configuration with a grid cell density of 200 and CFL number 0.05, has a very long computational time. The comparative graph presented in figure 3.15, shows convergence of the wave amplitude to the expected theoretical value on reduction of the CFL number from 0.5 to 0.05.

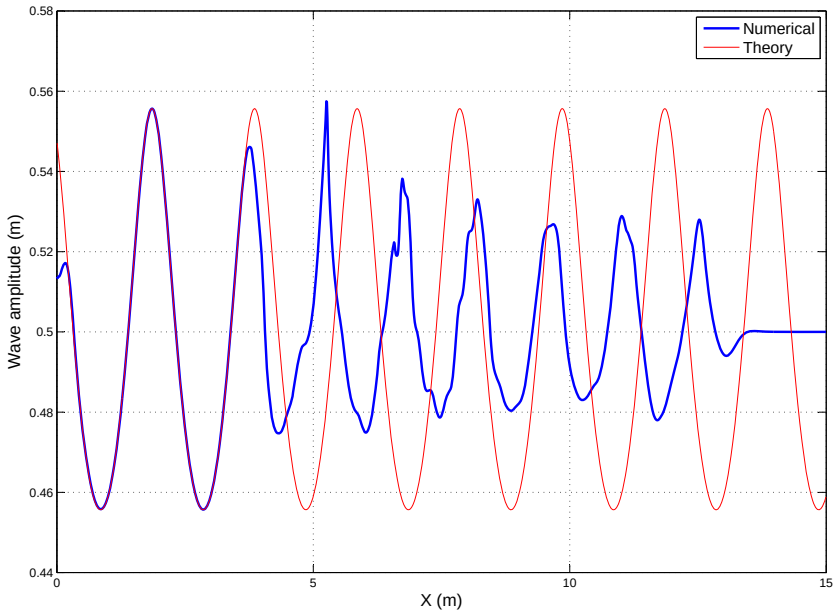

Figure 3.9: Solution with CFL number=0.5 (dx=0.01, a=0.05, λ=2.0m)

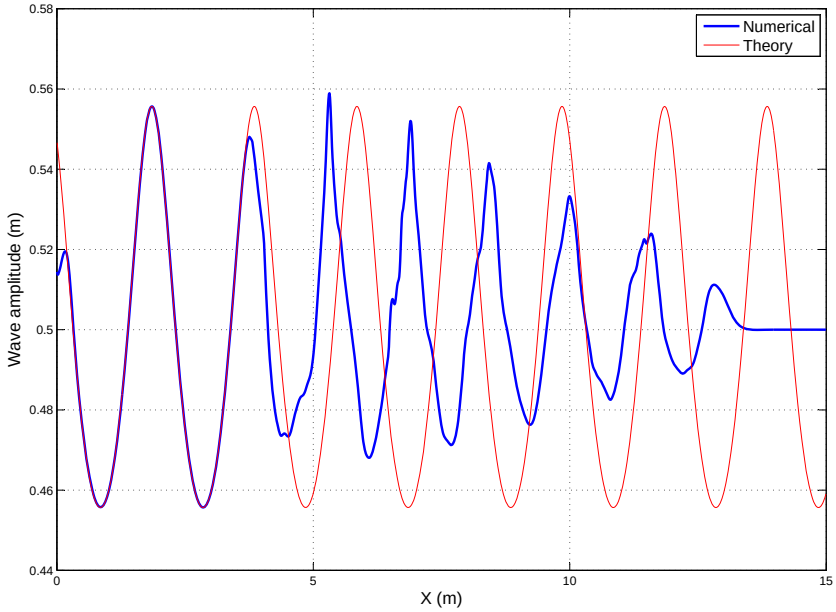

Figure 3.10: Solution with CFL number=0.4 (dx=0.01, a=0.05, λ=2.0m)

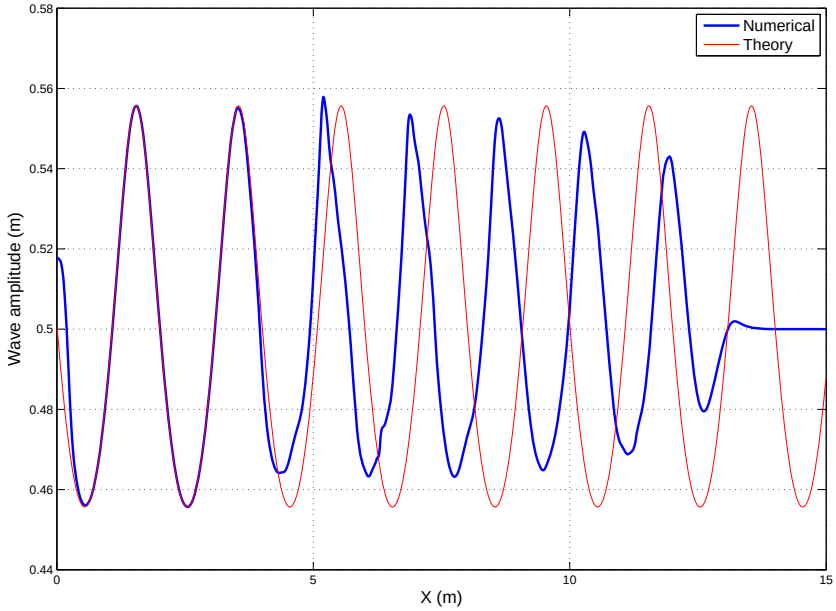

Figure 3.11: Solution with CFL number=0.3 (dx=0.01, a=0.05, λ=2.0m)

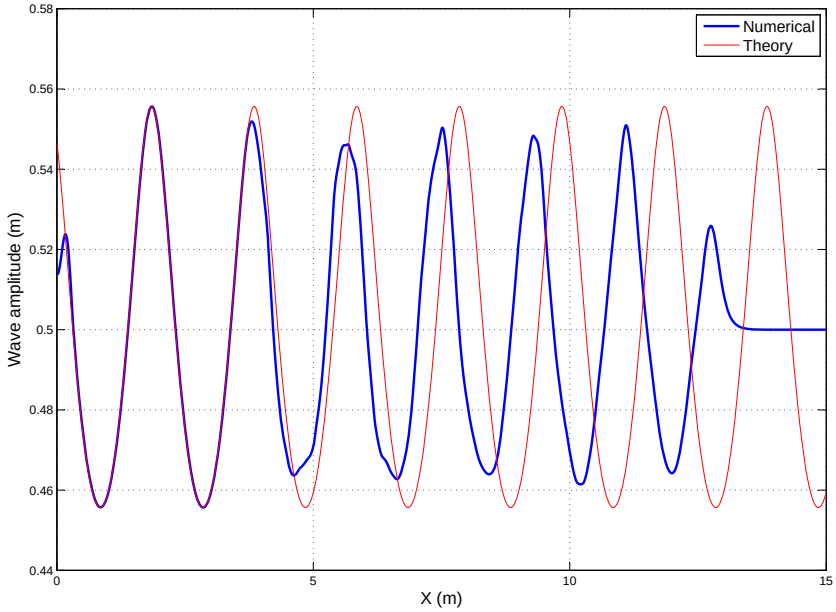

Figure 3.12: Solution with CFL number=0.2 (dx=0.01, a=0.05, λ=2.0m)

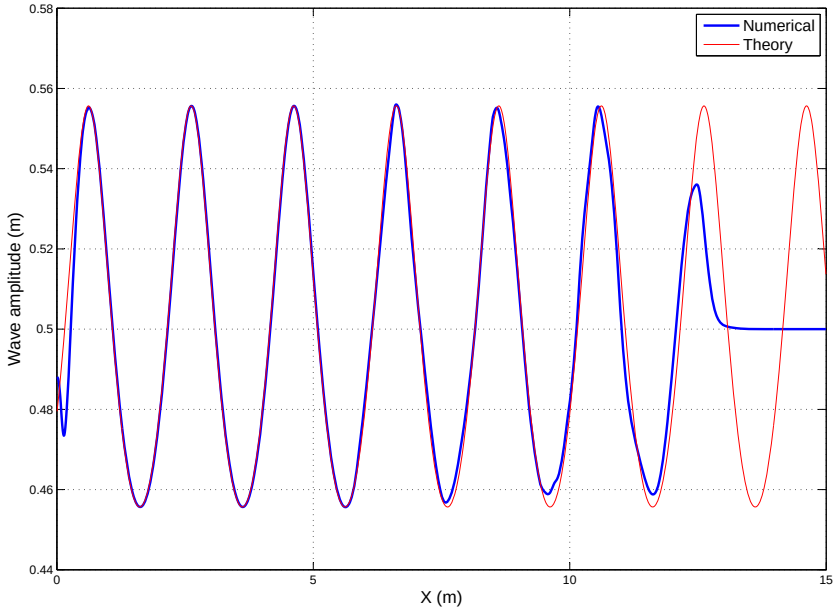

Figure 3.13: Solution with CFL number=0.1 (dx=0.01, a=0.05, λ=2.0m)

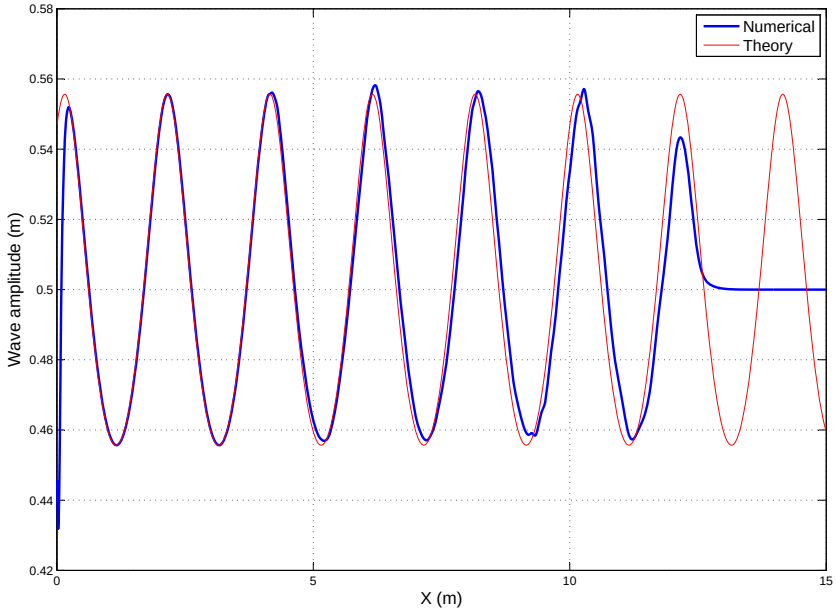

Figure 3.14: Solution with CFL number=0.05 (dx=0.01, a=0.05, λ=2.0m)

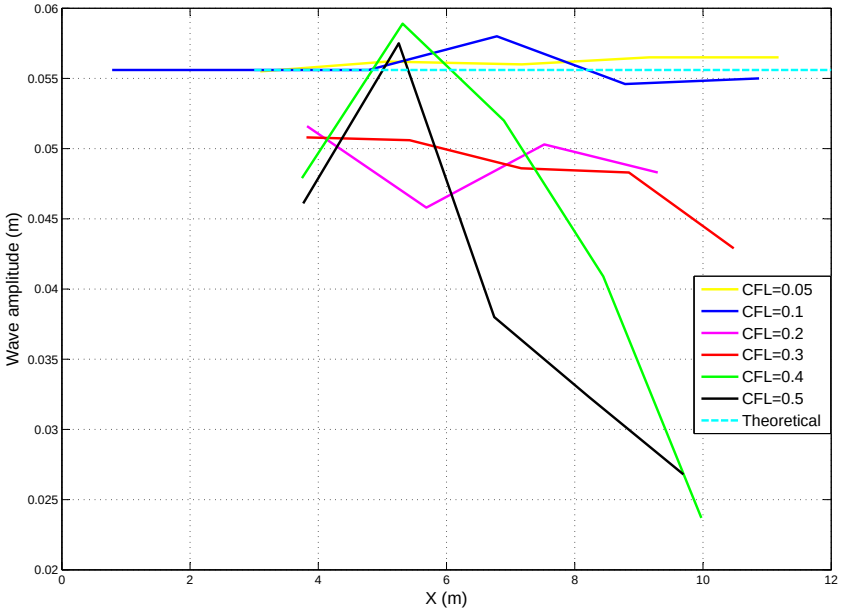

Figure 3.15: Convergence of wave amplitude on reduction of CFL number

3.3.3 Effect of length of the numerical beach

Dissipation of waves generated in the wave tank is an essential function to be taken care of during its development. The numerical beach, created for this purpose, should be long enough to be able to effectively absorb the incoming waves. The presence of a long beach may help in the dissipation of the waves, but will take up a large amount of space in the wave tank. Conversely, an inadequate length of the absorption zone will result in reflection from the boundary and pollute the numerical solution in the wave tank. So, it is necessary to determine the adequate length of the absorption zone. The trials in this section have been carried out with a fifth order Stokes wave with amplitude $0.05m$, wavelength $2.0m$ and grid size $0.01m$. WENO scheme and TVD 4^{th} order Runge-Kutta scheme are the spatial and time discretization schemes used in this trial. Solutions obtained over multiple wave periods are superimposed in the figures presented in this section, so as to visualize with more clarity, the effect of reflection over several wave periods. The boundary between relaxation zone 2 and the working zone of the tank is marked by a vertical dotted line.
Figure 3.16 presents the development of standing waves in the wave tank in the absence of a beach. The solutions for trials with beach length 0.5, 1.0, 2.0, and 3.0 times the wavelength respectively are presented in figures 3.17 through 3.20. It is observed that the increase in amplitude caused by reflection from the boundary is reduced with the increase in beach length.
A plot of the maximum heights of the crests and the maximum depths of the troughs observed in figures 3.17 to 3.20 is presented in figure 3.21. This is done to visualize the effect of increasing beach width on the wave amplitude error caused by reflection. From this figure, the convergence of the wave amplitude towards the expected theoretical values can be seen with increase in beach width. It is noticed that increasing the beach width beyond two times the wavelength does not seem to have a visible effect on the results. This conforms with the rule of thumb suggested in[9], mentioned in section 3.1.2.

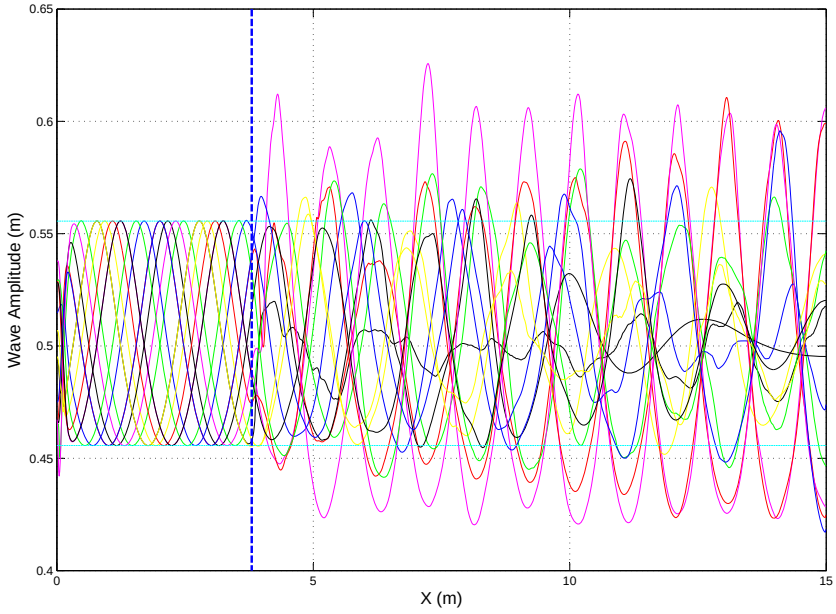

Figure 3.16: Solution in the absence of numerical beach (a=0.05, λ=2.0m)

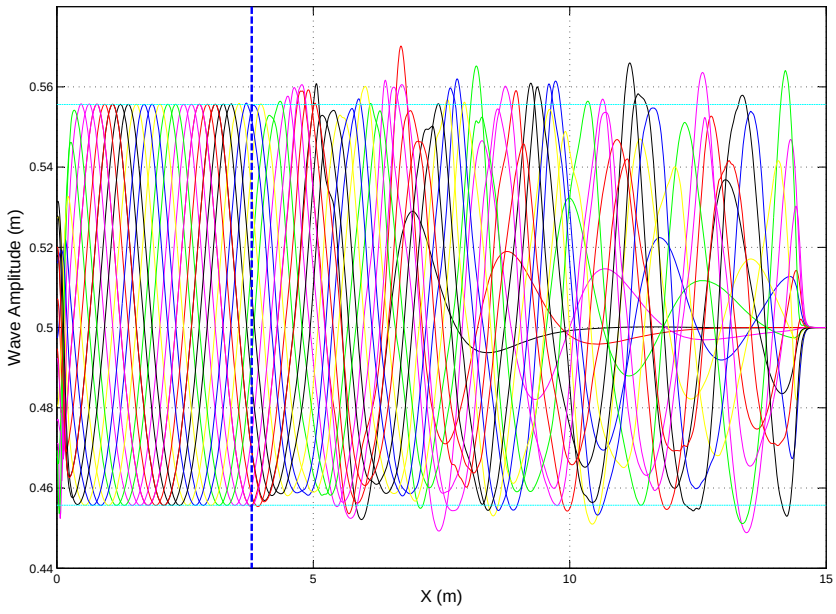

Figure 3.17: Solution with a numerical beach of length 1m (a=0.05, λ=2.0m)

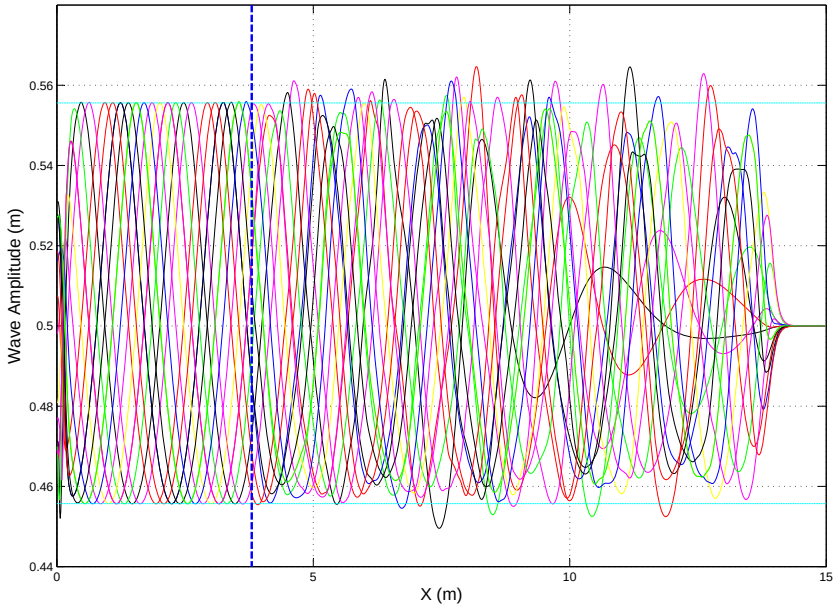

Figure 3.18: Solution with a numerical beach of length 2m (a=0.05, λ=2.0m)

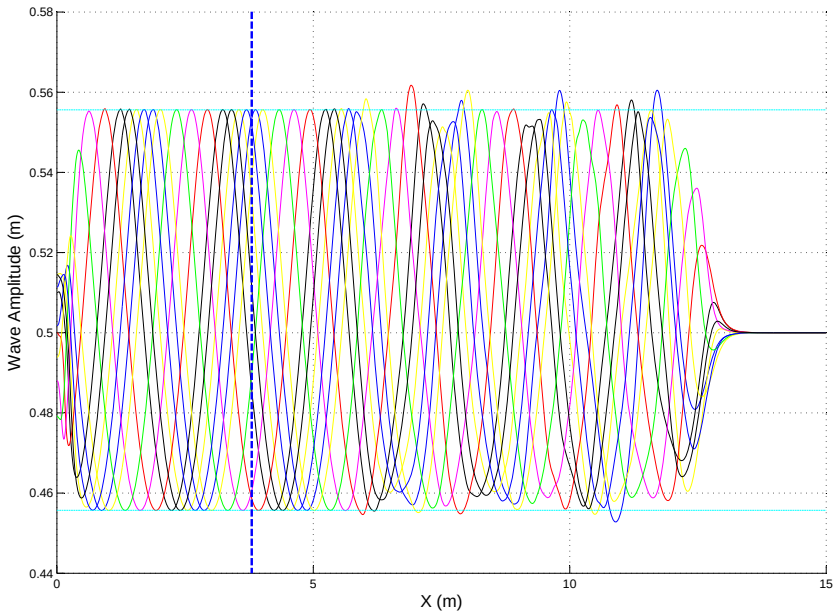

Figure 3.19: Solution with a numerical beach of length 4m (a=0.05, λ=2.0m)

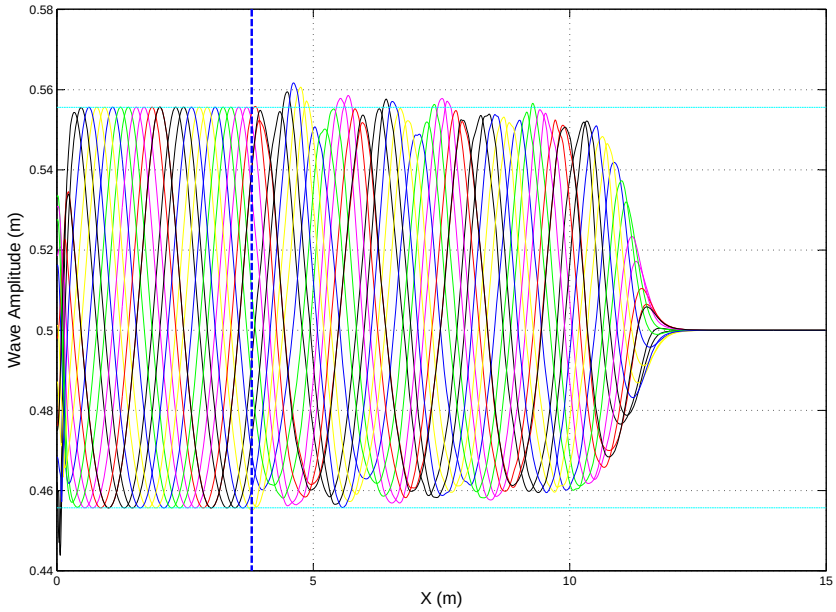

Figure 3.20: Solution with a numerical beach of length 6m (a=0.05, λ=2.0m)

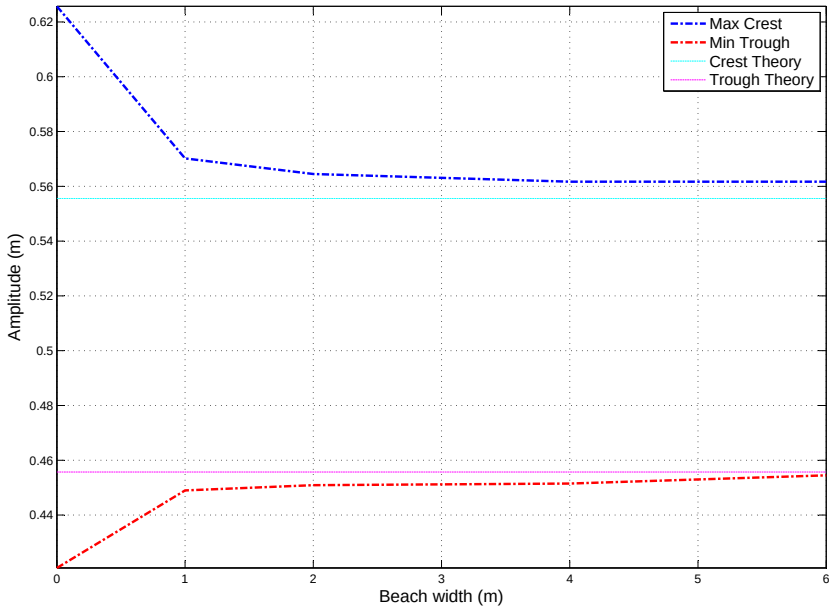

Figure 3.21: Convergence of amplitude maxima and minima to the theoretical on increase of beach width (a=0.05, λ=2.0m)

3.3.4 Performance of different convection discretization methods

Different convection discretization schemes for the momentum equation and the level set function that can be utilized for numerical simulations employing the finite difference methods were described in section 2.2.1. This set of trials explores the solutions obtained using the WENO, TVD and SMART schemes using a wave of amplitude $0.05m$, wavelength $2.0m$ and grid size of $0.01m$. The 4^{th}order Runge-Kutta time discretization is followed for all these trials.

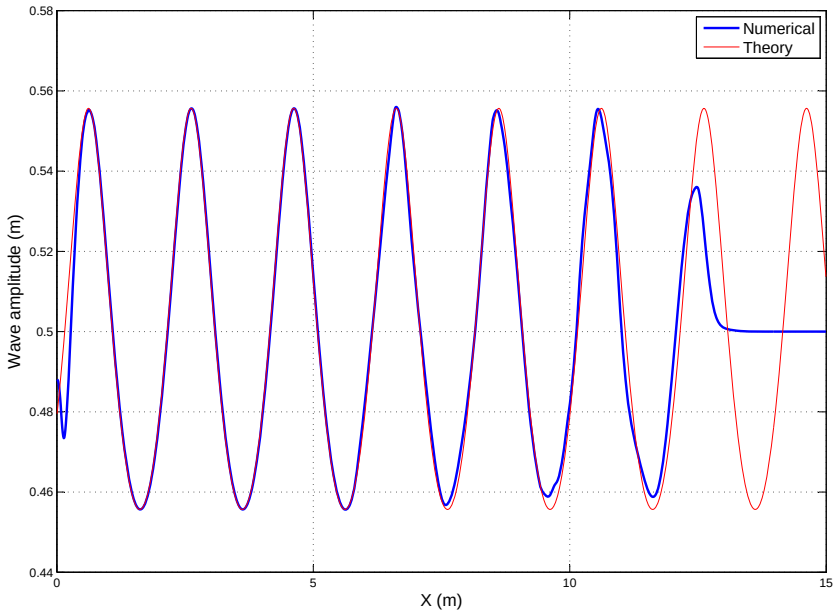

Figure 3.22: Solution using the WENO scheme

From the figures presented for this set of trials, it can be noticed that the results of the SMART scheme are comparable to the results from the WENO scheme except for a few wiggles in some parts of the solution. The solution obtained using the TVD scheme results in a reduction of the wavelength as the wave exits the relaxation zone 2 and propagates through the working zone of the wave tank.

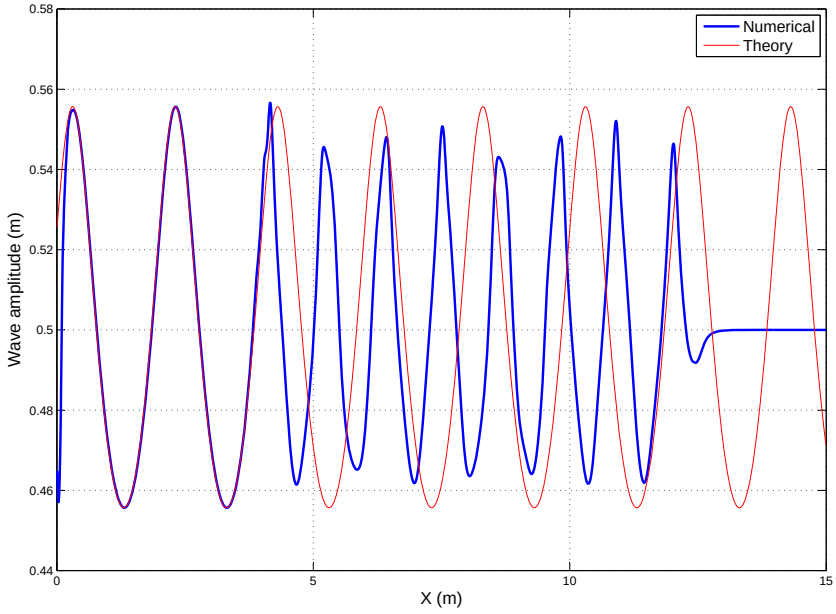

Figure 3.23: Solution using the TVD scheme

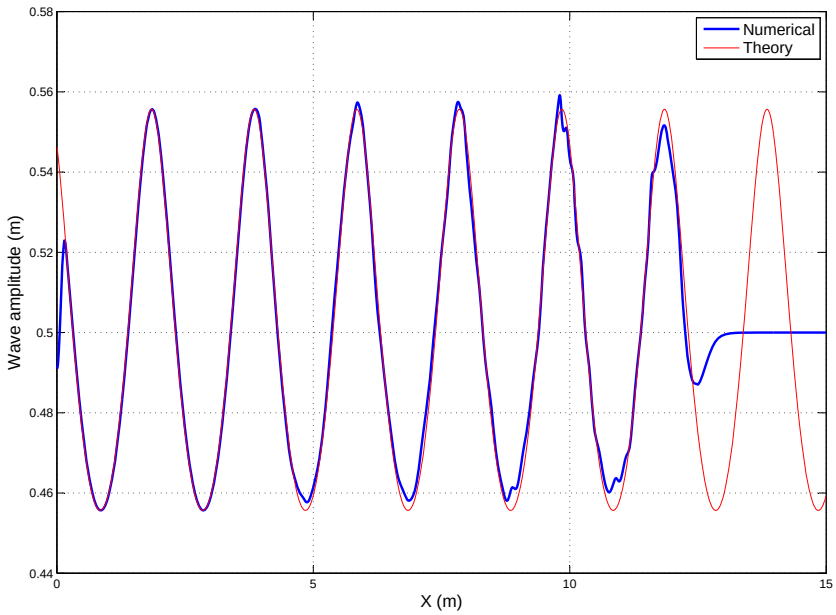

Figure 3.24: Solution using the SMART scheme

3.3.5 Performance of different time discretization methods

The effect of higher order time discretization of the momentum equation and the level set function is explored in this set of tests. The time discretization schemes described in section 2.2.2 are employed to observe the difference in the solution among methods with second, third and fourth order time discretization schemes. Figures 3.25, 3.26 and 3.27 below are the results obtained for the Adam-Bashforth and TVD 3^{rd} and $4th$ order Runge Kutta schemes respectively. The WENO scheme is employed for the convection discretization in all these trials. A fifth order Stokes wave with amplitude $0.05m$, wavelength $2.0m$ and grid size $0.01m$ is used in this section.

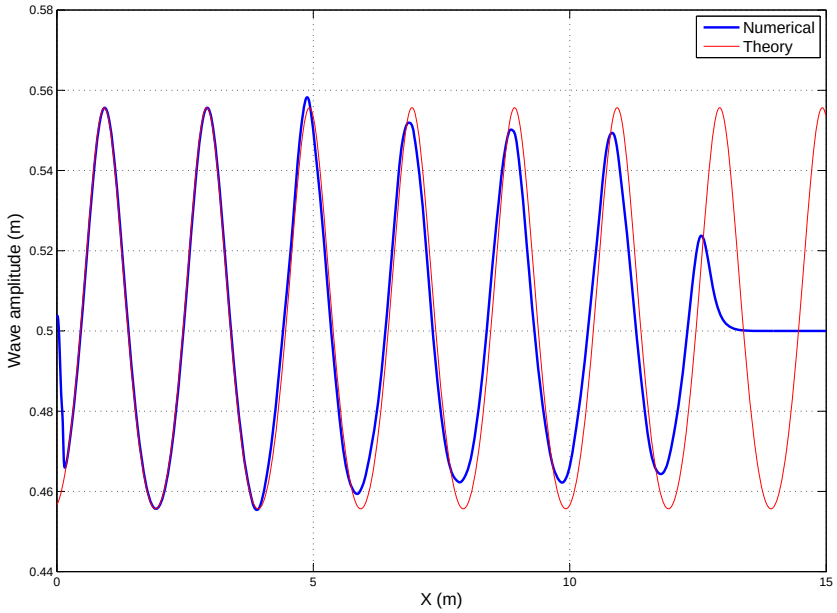

Figure 3.25: Solution using the Adam-Bashforth scheme

The 4^{th} order Runge Kutta scheme is seen to perform well. Agreement of wave phase is seen to be better in the Adam-Bashforth method whereas the agreement in amplitude is observed to be better in the 3^{rd} order Runge Kutta scheme.

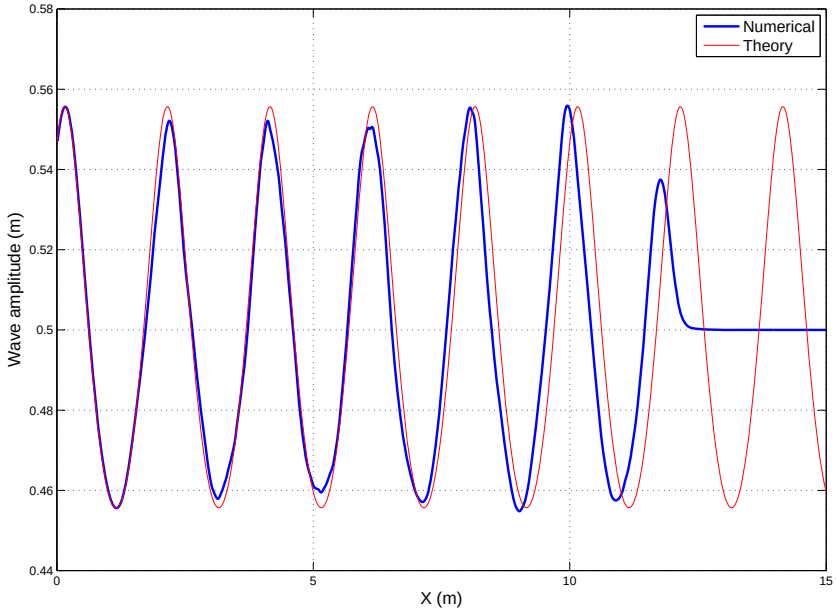

Figure 3.26: Solution using the 3^{rd} order Runge-Kutta TVD scheme

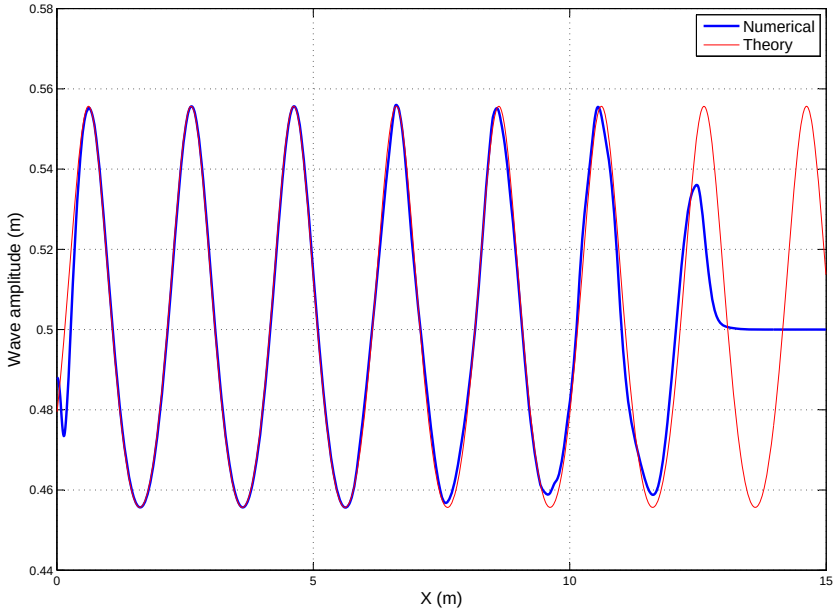

Figure 3.27: Solution using the 4^{th} order Runge-Kutta scheme

3.3.6 Performance under different relaxation methods

Two relaxation methods were presented in section 3.1.2. The performance of these two methods are tested. A fifth order stokes wave of amplitude $0.05m$ and wavelength $2.0m$ with a water depth of $0.5m$ is used here. From the figures 3.28 and 3.29 it is observed that the effect of reflection in the Jacobsen method is comparatively more than that seen in the Engsig-Karup relaxation method.

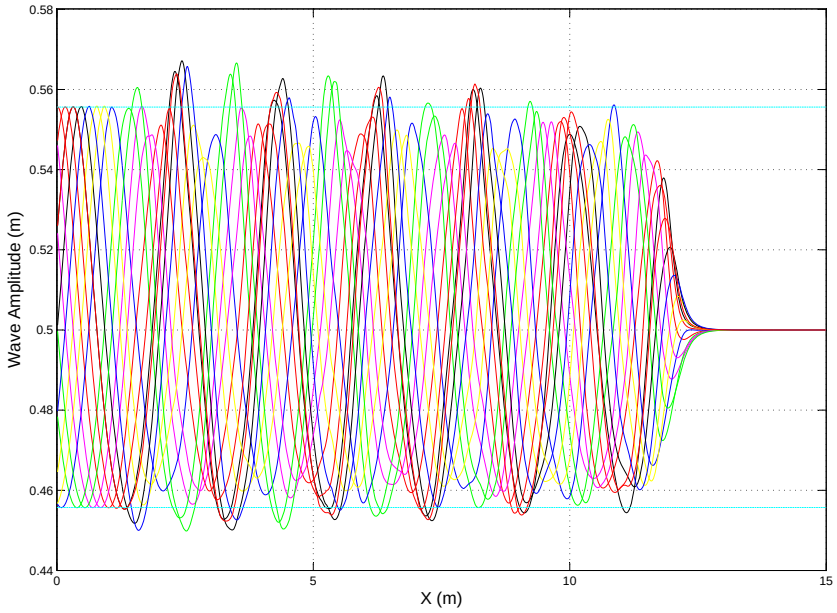

Figure 3.28: Solution using the Jacobsen relaxation method

A feature to be noted in this case is that the Jacobsen method of relaxation does not consist of a second relaxation zone (zone 2) unlike in the Engsig-Karup method. This could be one of the reasons for the increased reflective action, with reflected waves travelling between the inlet and outlet boundaries.

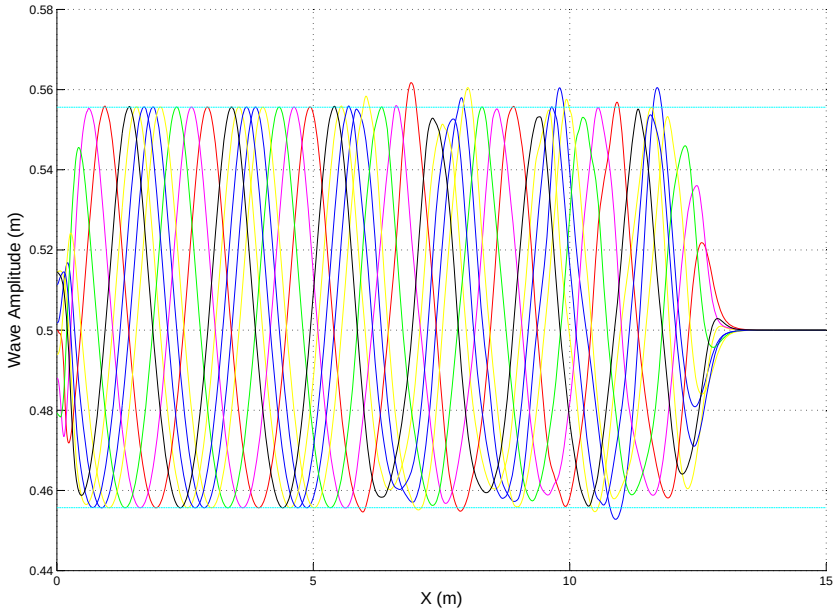

Figure 3.29: Solution using the Engsig-Karup relaxation method

3.3.7 Performance at different amplitudes

The performance of the wave tank for different wave amplitudes, in accordance to the limitations of the wave theory used, was tested. The following figures are the results obtained for the wave amplitudes $0.01m$, $0.03m$, $0.05m$ *and* $0.07m$ at a water depth of $0.5m$ for a wavelength of $2.0m$. The grid size is $0.01m$ and CFL number=0.1. The WENO scheme and 4^{th} order Runge-Kutta scheme are used for the convection and time discretizations respectively.
A point of interest in figure 3.30 is the slight reduction in amplitude with the progression of the wave. This could be intuitively attributed to insufficient cell density in terms of the amplitude. Other than cell density, there are two other aspects in the numerical wave tank, which seem to effect the solution. The first aspect is the phenomenon of the smaller wave created due to still water encountered by the wave mentioned in section 3.3.1. This effect is seen to slowly wear off once the wave establishes itself in the tank, after a few wave periods. The second aspect is the reflection from zone 3. For waves of higher amplitudes, the reflection causes a few crests to deviate from the theoretically expected value as seen in figures 3.32 and 3.33. At a lower amplitude of say $0.03m$, the reflected wave seems to of high frequency and causes the wiggles seen in fig 3.31. Overall, from this section, the wave tank seems to show better performance at higher amplitude.

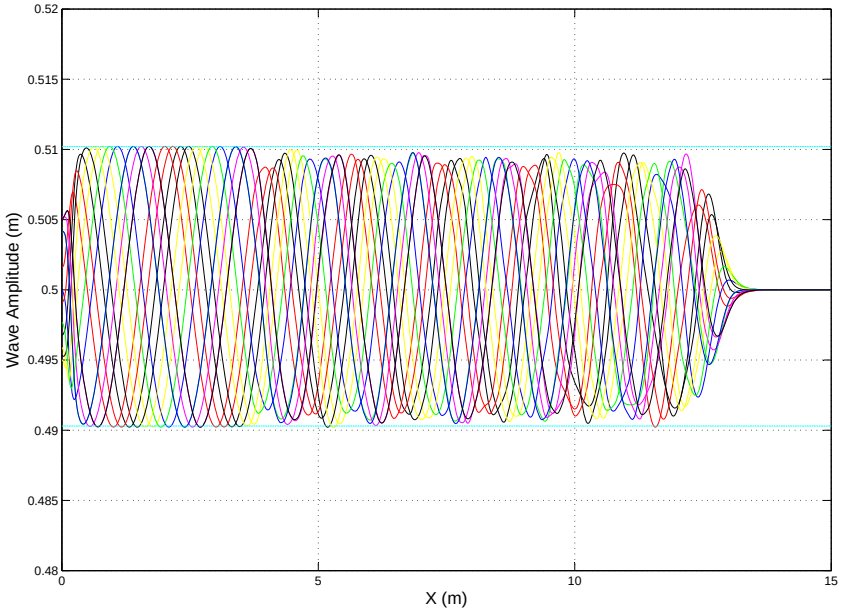

Figure 3.30: Solution for a wave amplitude of 0.01m

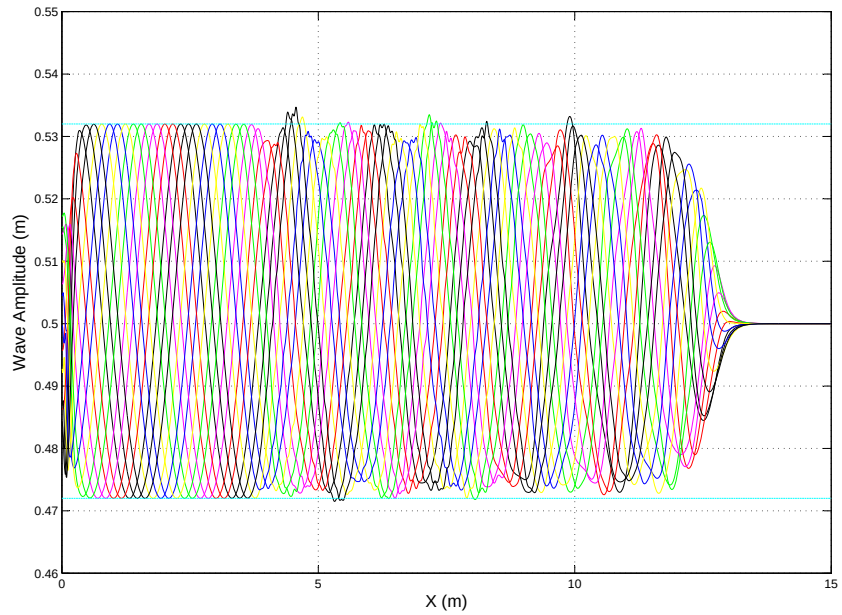

Figure 3.31: Solution for a wave amplitude of 0.03m

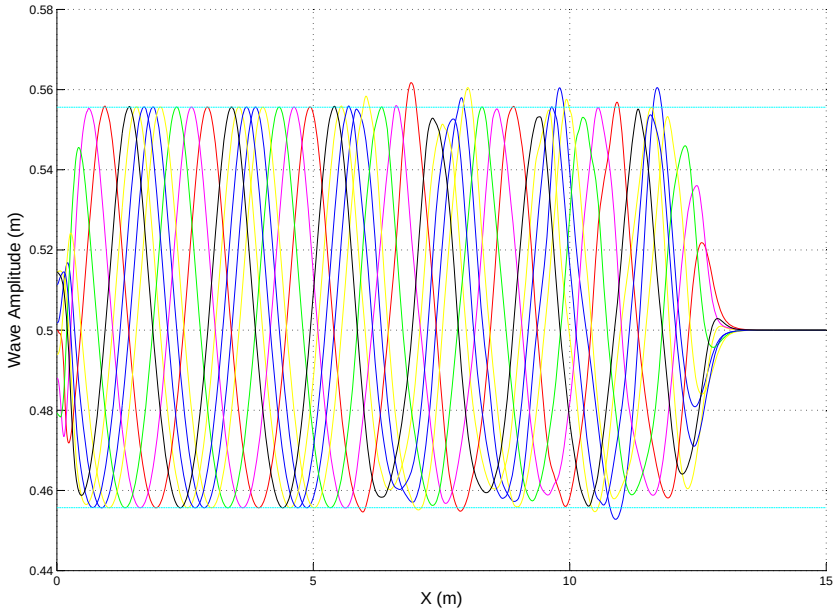

Figure 3.32: Solution for a wave amplitude of 0.05m

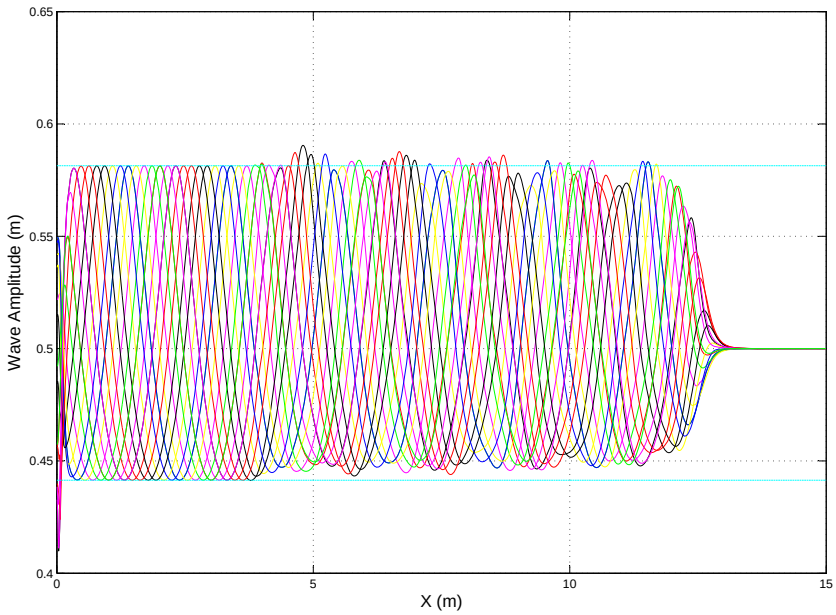

Figure 3.33: Solution for a wave amplitude of 0.07m

3.3.8 Performance of different wave types

REEF3D is capable of generating waves conforming to many wave theories. The results for waves generated using the linear wave theory, second order stokes and the fifth order stokes wave theories are presented in the figures below. Waves with varying amplitudes and types of wavelength $2.0m$ are generated with a grid size of 0.01m. WENO scheme and 4^{th} order Runge-Kutta scheme are employed for spatial and time discretization respectively.

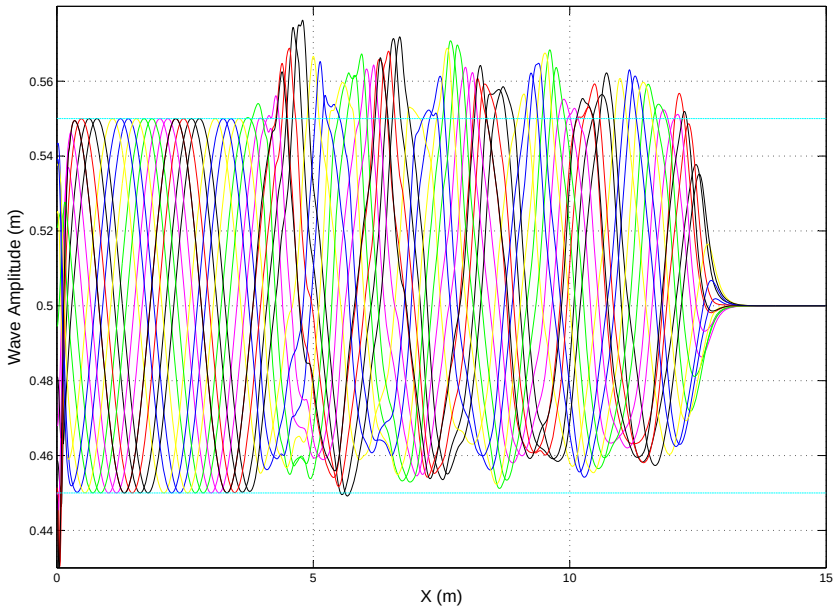

Figure 3.34: Simulation of linear waves with amplitude 0.05m

In figures 3.34 and 3.36, the solutions for first order and second order waves respectively with wave amplitude of $0.05m$ are presented. An interesting observation is that the effect of reflection is considerably more in these cases than at a lower amplitude as seen in figures 3.35 and 3.37. These effects are much lesser in the fifth order Stokes wave presented in figures 3.38 and 3.39.

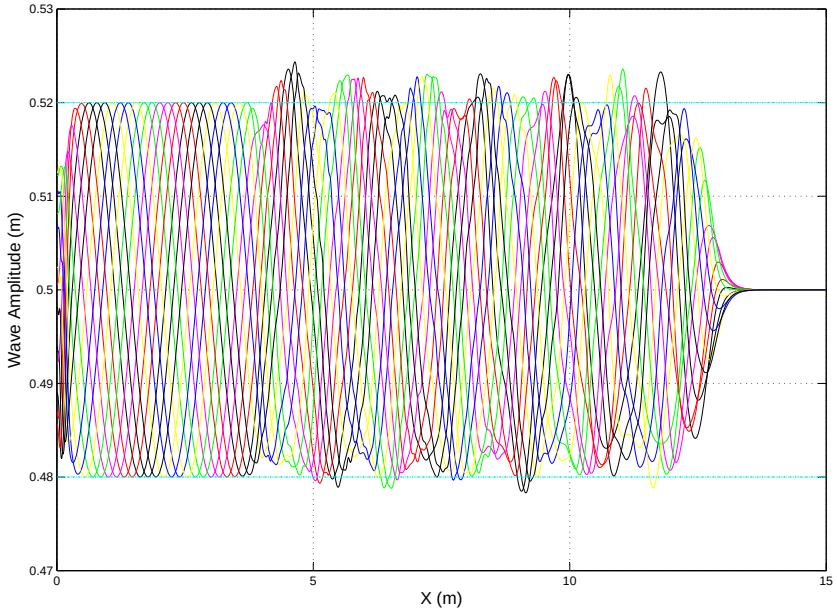

Figure 3.35: Simulation of linear waves with amplitude 0.02m

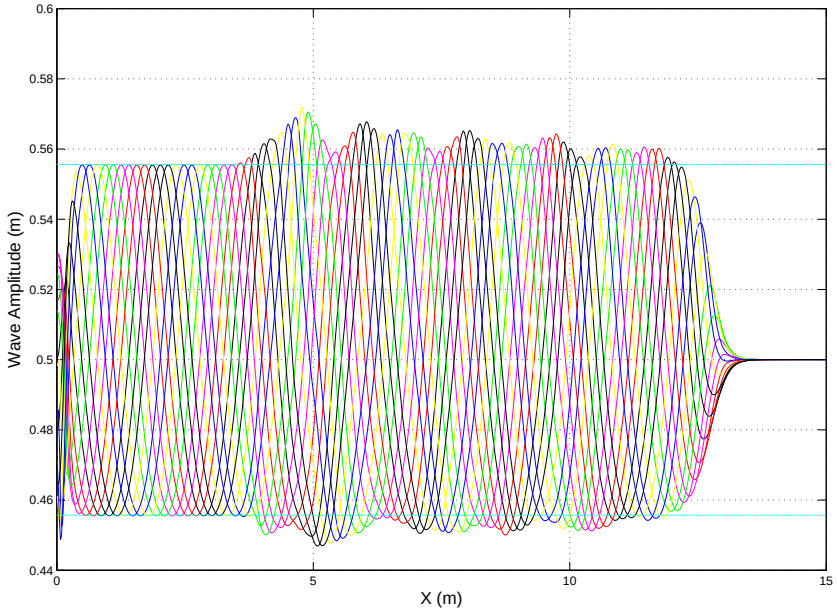

Figure 3.36: Simulation of second order Stokes waves with amplitude 0.05m

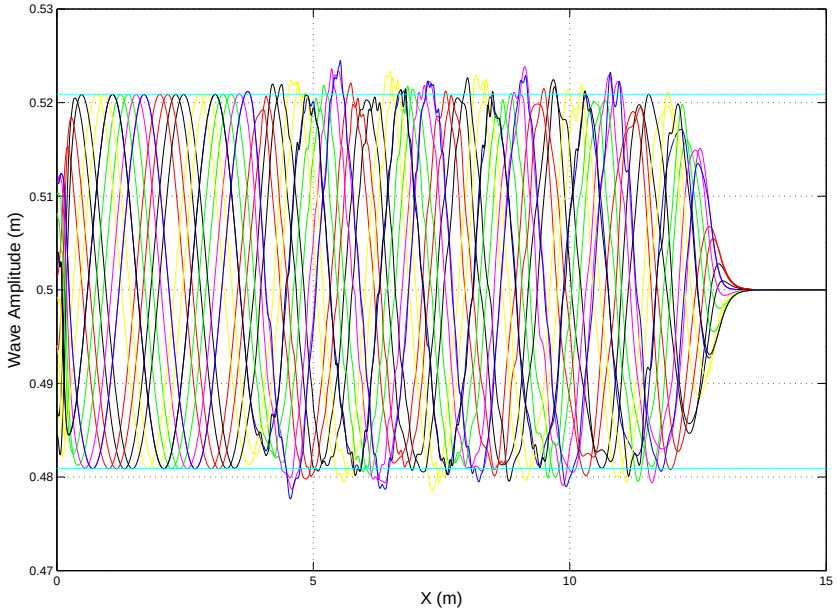

Figure 3.37: Simulation of second order Stokes waves with amplitude 0.02m

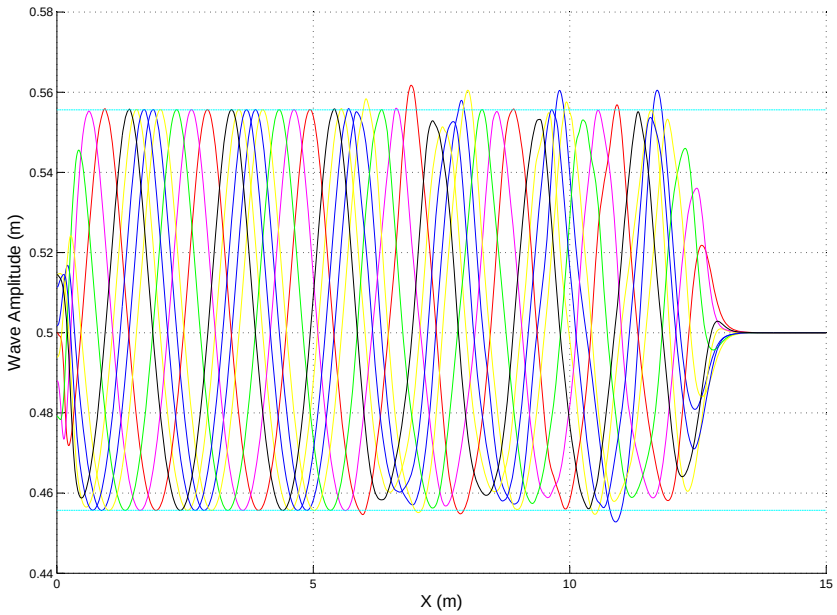

Figure 3.38: Simulation of fifth order Stokes waves with amplitude 0.05m

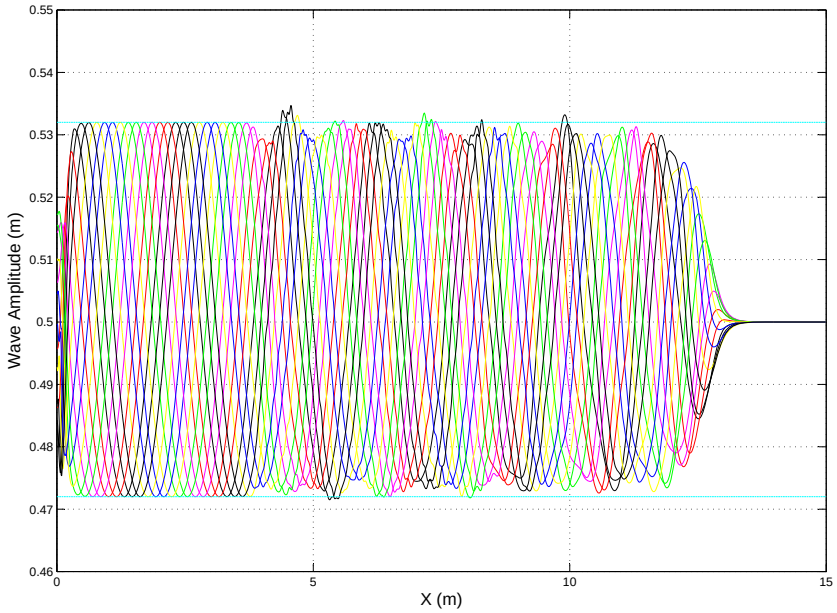

Figure 3.39: Simulation of fifth order Stokes waves with amplitude 0.03m

Chapter 4

Wave Forces

4.1 Wave Forces on Structures

In civil engineering, calculation of forces on structures forms an important part of any work because having a good idea of the forces to be withstood by the structure leads to a sound, safe and economical design. Wave forces on structures are calculated under different scenarios, depending on the type of waves encountered− breaking or non-breaking; dimensions of the structure− slender or large; and type of flow regime− separated or non-separated. The Reynolds number associated with the flow also becomes an important factor as it determines flow regime and the type of relation that exists between the flow and the force exerted by it on the structure. Two other important parameters in this subject are the Strouhal number and the Keulegan-Carpenter number.
The Keulegan-Carpenter number, KC, is a non-dimensional parameter which indicates the flow regime in an oscillatory flow as a function of the wave amplitude, wave period and diameter of the cylinder, where:

$$KC = \frac{a\,T}{D} \tag{4.1}$$

The Strouhal number, S_0, is another dimensionless parameter that is an indicator of the flow regime in case of flow separation and vortex formation. It is a function of the vortex shedding frequency, cylinder diameter and the flow velocity such that:

$$S_0 = \frac{f_0 D}{U} \tag{4.2}$$

Froude-Krylov Force

The first concept to be looked at while studying wave forces on structures is the calculation of the Froude-Krylov force. This is the force exerted by the fluid in an

undisturbed wave field, that is, when the structure is considered to be transparent to the wave. This is calculated by integrating the pressure around the cylinder as

$$f_{FK} = \rho \left(\frac{\pi D^2}{4} \right) \dot{U} \tag{4.3}$$

This is actually an application of the Newton's second law with the mass of the 'transparent' cylinder being equal to the mass of the water displaced by it and on multiplication of the acceleration of the fluid, one obtains the force acting on the surface.

Form Drag Force

A structure that is inserted normal to the current in a steady flow is subjected to a frictional force as it acts as an obstacle in the flow regime. This frictional force is referred to as the form drag force, calculated per unit length of the cylinder as

$$f_d = \frac{1}{2} \rho C_d D U |U| \tag{4.4}$$

The modulus around the velocity term in the above equation serves the purpose of preserving the direction of the velocity as the force acts in the same direction as the velocity of the fluid. The term C_d is a dimensionless parameter known as the drag force coefficient which is a function of the Reynolds number defined as

$$Re = \frac{UD}{\nu} \tag{4.5}$$

The above relation in eqn. (4.4) is applicable under steady flow regimes, where the flow properties are considered to be stationary. Also, as an extension, in case of flow separation with high vortex shedding frequency, the flow regime can be deemed quasi-steady and the same relation holds.

4.1.1 Potential Theory for Slender Cylinders

A cylinder is termed a slender cylinder when its diameter is small compared to the wavelength, in principle, $\lambda/D > 5$. Under this condition, the cylinder is considered to be small enough such that the flow regime is not disturbed to the extent of causing flow separation downstream of the cylinder.
The potential theory is a first order theory, based on the linear wave theory and the solutions are accurate to the first order. This is used to calculate the non-breaking wave force on a slender cylinder. The concept of the Froude-Krylov force represented in equation (4.3) is to be extended to account for the presence of the cylinder, which in

reality, disturbs the wave field. The solution to be found now, for an incompressible, inviscid fluid in irrotational flow has to follow the following conditions:

- Satisfy the Laplace equation, $\nabla^2\Phi = 0$
- Particle velocities normal to the body must be zero, $\partial\Phi/\partial n = 0$
- The undisturbed velocity potential is restored at a distance far away from the cylinder.

The above conditions can be satisfied by introducing a 'diffraction potential'. The total velocity potential is then the sum of this added term and the original velocity potential. But due to the assumption of a slender cylinder the diffraction term of the diffraction potential is considered negligible in comparison to the undisturbed velocity potential. On integrating the dynamic pressure so obtained from the simplified new velocity potential, the net force acting on the cylinder is found to be

$$f = 2\rho\left(\frac{\pi D^2}{4}\right)\dot{U} \tag{4.6}$$

It is seen that this is exactly twice the Froude-Krylov force. The force calculated in eqn. (4.6) can be decomposed into two parts as

$$f = \rho\pi\frac{D^2}{4}\dot{U} + \rho C_a\pi\frac{D^2}{4}\dot{U} \tag{4.7}$$

The first term is the Froude-Krylov force from eqn. (4.3). The second term is the hydrodynamic mass force which comes into play as the fluid particles around the cylinder are accelerated as the cylinder moves under the influence of the fluid pressure acting on it. For a slender cylinder, the added mass coefficient, $C_a = 1$. The relation in eqn. (4.7) can thus be written as

$$f = (1 + C_a)\rho\pi\frac{D^2}{4}\dot{U} = C_m\rho\pi\frac{D^2}{4}\dot{U} \tag{4.8}$$

For a slender cylinder, as can be observed from eqn. (4.8), $C_m = 2$.

4.1.2 MacCamy Fuchs Theory

The wave forces explored in sections 4.1.1 and 4.1.3 were approximated under the assumption of a slender cylinder. In cases where the cylinder does not obey the criterion

of being slender, a different approach is required as the wave undergoes scattering on encountering the structure. A first order theory extended to intermediate depths, based on the potential theory was proposed in 1954 by MacCamy and Fuchs[21]. The diffraction term in the diffraction potential as introduced in section 4.1.1 cannot be neglected in this case and is represented by the use of an infinite series of Bessel functions. The dynamic pressure is determined again and integrated around the cylinder to obtain the net force in the direction of wave propagation as

$$\begin{aligned} f_x = \frac{2\rho g H}{k_f} \frac{cosh\ k_f z}{cosh\ k_f d} \frac{1}{\sqrt{A_1(k_f a)}} cos(\omega_f t - \alpha) \\ where,\ A_1(k_f a) = {J_1'}^2(k_f a) + {Y_1'}^2(k_f a) \\ and\ \alpha = tan^{-1}\left(\frac{J_1'(k_f a)}{Y_1'(k_f a)}\right) \end{aligned} \tag{4.9}$$

The terms J and Y used in the above equation are Bessel functions.

4.1.3 Morison Formula

The presence of a structure in a wave field gives rise to complex flow patterns depending on the Reynolds number of the flow. In some scenarios, after the passage of a certain amount of time, the flow pattern changes and gives rise to a phenomenon called vortex shedding. This is a process by which a boundary layer of the flow separates from the main streamlines around the cylinder rolls up and forms vortices. These vortices stay behind the cylinder initially and then are shed alternatively into the flow behind the cylinder. Thus, the forces acting on the cylinder are not only dependent on the velocity field but also on the flow history. Under circumstances where the flow is steady and there is no formation of vortices, potential theory gives a good representation of the hydrodynamics around the cylinder as expressed in section 4.1.1. Also, production of a large number of vortices in half a flow cycle, the flow regime can be assumed to be quasi-steady and a good approximation be obtained by calculating the drag force as described in section 4.1. A flow regime lies between these two cases of flow without vortices and with high vortex generation rate with both acceleration of the structure and flow separation. The Morison equation is an empirical formula that is used to evaluate the wave forces on the cylinder in this flow regime.

According to the Morison equation the force on the cylinder can be calculated as the sum of the inertia forces and the form drag on the cylinder. Each of the two terms are then adjusted with force co-efficients C_m and C_d to obtain the force per unit length as

$$f = \frac{1}{4} C_m \pi D^2 \rho \dot{U} + \frac{1}{2} C_d \rho D U |U| \tag{4.10}$$

It has to be noted that the force coefficients C_d and C_m used above are not the same as the coefficients encountered in section 4.1 with the Froude-Krylov and form drag forces. The values of the experimentally determined coefficients here are obtained from charts which plot their values against the Reynolds number for various values of the Keulegan Carpenter number, KC.

4.2 Method for calculation of forces in REEF3D

The general idea behind the evaluation of wave forces in sections 4.1.1 through 4.1.2 is to integrate the pressure around the cylinder. This study uses the same concept in for numerical calculation of wave forces. The numerical model provides a very accurate description of the surface profile and this is utilized to calculate the pressure around the cylinder.
In the model, the pressure and shear stress around the boundary of the cylinder are integrated as illustrated in figure 4.1. Mathematically, the surface normal vectors are produced for the pressure and the shear force around the cylinder and the sum of these integrated over the surface of the cylinder. This can be represented in an equation as,

$$F = \int_{\Gamma} (-\mathbf{n}p + \mathbf{n}.\tau) d\Gamma \tag{4.11}$$

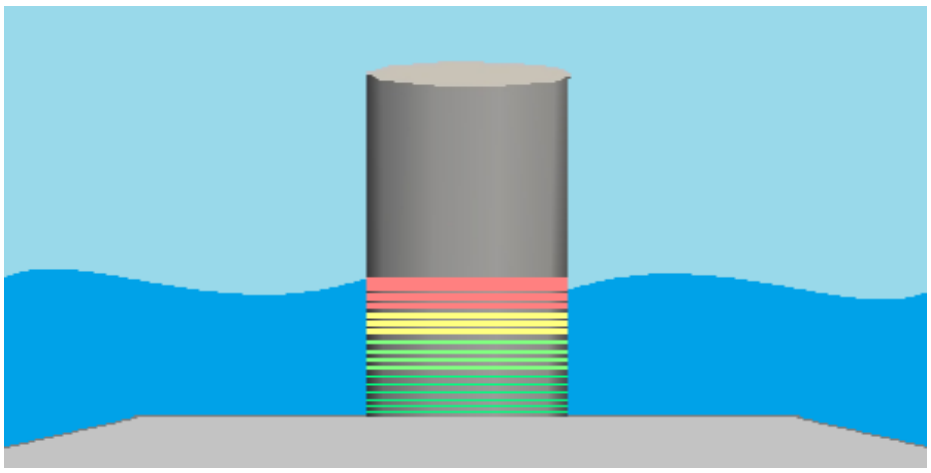

Figure 4.1: Calculation of wave forces by integration of pressure and shear force

4.2.1 Calculation of Morison Force

The Morison formula is used in order to compare the numerical results obtained with the theoretically expected values. This formula described in section 4.1.3, uses two experimentally determined variables C_d and C_m.
The values for these coefficients are evaluated from the charts which plot their variation against the Re and for different values of KC. To effectively compare the theoretical value with the numerical solution, the Morison formula has to be evaluated at every time step. In order to do this, the charts for these coefficients are digitized and curve fitting is carried out. The curve fitting tool available in Matlab is employed for this purpose. Polynomial fits of the sixth, seventh and eighth order are tried and the curve with a coefficient of determination (R^2) more than 0.96 and the best visual fit is chosen. An example is shown in figure 4.2, for KC=40. The equation obtained for this curve is an eighth degree polynomial:

$$C_d = 2.48e-46 * Re^8 - 1.277e-39 * Re^7 + 2.762e-33 * Re^6 - 3.263e-27 * Re^5$$
$$+2.29e-21 * Re^4 - 9.706e-16 * Re^3 + 2.406e-10 * Re^2 - 3.133e-5 * Re + 2.185.$$

This process is carried out for C_d and C_m curves for KC numbers 6, 8, 10, 15, 20, 40, 60 and 100. The curves presented in [29] are used in this study.
Values of velocity and acceleration, required for force calculation are obtained from the wave tank as follows. An average velocity is calculated using the velocities on either side of the pier, along the red lines illustrated in figure 4.3. This is used in the part of the formula that accounts for the drag force. The gradient of the velocity over a time step is then calculated and used as the acceleration in the inertial force part of the formula. This method of calculating the acceleration can give rise to some shocks in the solution, resulting in jumps in the solution for the inertial force. A filter can then be applied to smoothen the solution. It is important to note that the jumps occur in the calculation of the theoretical force and not from numerical instabilities during force calculation by REEF3D.

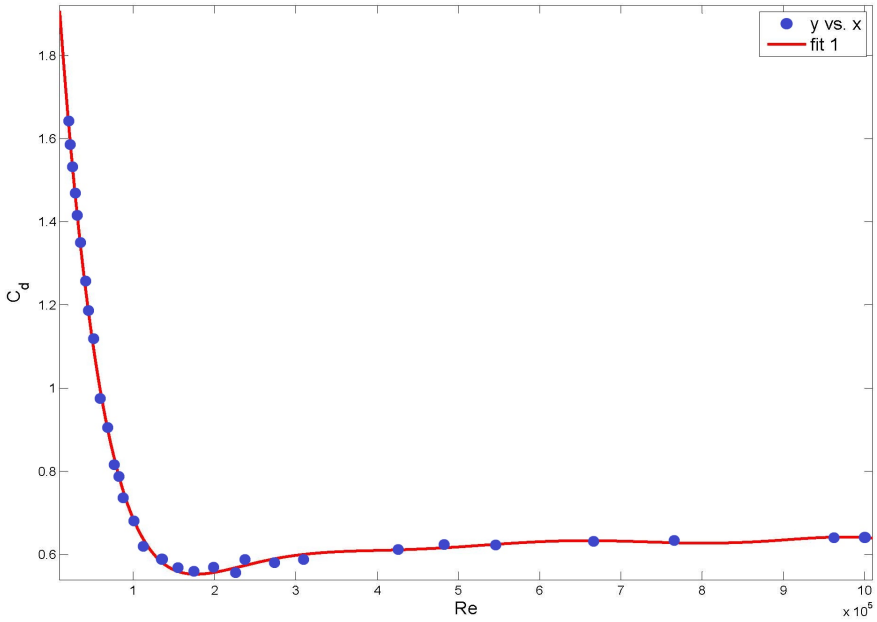

Figure 4.2: Curve fitting in Matlab for C_d at $KC = 40$

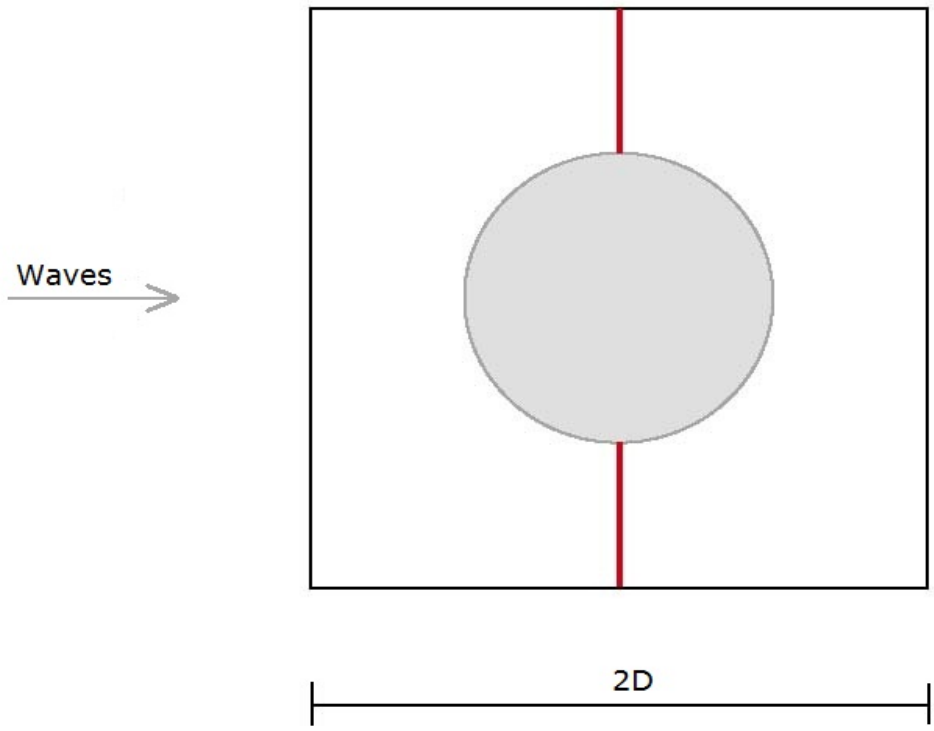

Figure 4.3: Calculation of average velocity for Morison formula

4.3 Results of wave force calculation

Wave force on a cylindrical pile of with diameter $0.2m$ are calculated for two setups, each with a coarse grid ($dx = 0.05m$) and a finer grid ($dx = 0.025m$). The first setup consists of a fifth order Stokes wave with an amplitude of $0.05m$, water depth $0.4m$ and wavelength $1.0m$ in a 3-dimensional numerical wave tank that is $10.0m$ long, $1.0m$ wide and $0.8m$ deep. The second setup simulates a fifth order Stokes wave with amplitude $0.075m$, water depth $0.4m$ and wavelength $2.0m$ in a wave tank $15.0m$ long, $1.0m$ wide and $0.8m$ deep. WENO scheme is used for spatial discretization and $4th$ order Runge-Kutta scheme is used for time discretization. The turbulence is calculated using the Wilcox's $k - \omega$ model in both the experiments.
The three-dimensional visualization of the numerical experiment is presented in figures 4.4 through 4.6 below. The elaborate representation of the free surface using CFD calculation can be seen in these images.

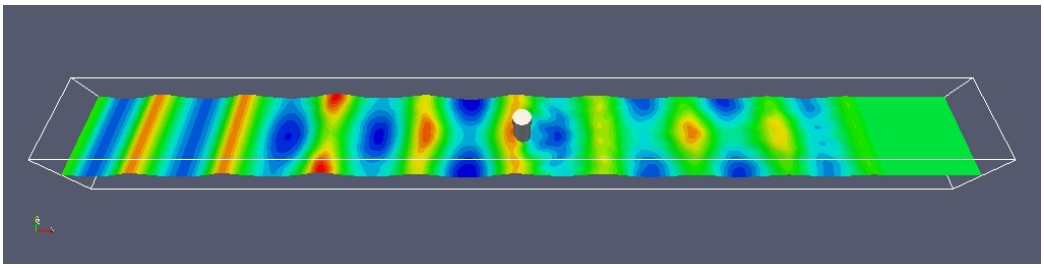

Figure 4.4: Visualization of the three-dimensional numerical wave tank

4.3.1 Coarse grid experiments

The first set of trials for force calculation is carried out on a coarse grid with $dx = 0.05m$ in The results of this trial are presented below. It is observed that, as discussed in section 4.2.1, there are a few jumps at a few points in the calculation of the theoretical force using the Morison formula (Figure 4.7). The force calculated by REEF3D does not show any effects of numerical instability in the solution. The theoretical results are then filtered to remove the spikes (Figure 4.8). The comparison of the filtered theoretical result with the numerical result for first wave setup is presented in figure 4.9. It is noted that the maximum amplitude of the force obtained numerically is less than the theoretical calculation. On an average, the difference between the numerical and theoretical result is 25%. It is worth recalling, at this point, the conclusion of section 3.3.1 that a higher grid density provides a better solution. From this finding, the error seen in the results here may be attributed to the lower grid density of 20 cells per wavelength available during this trial.

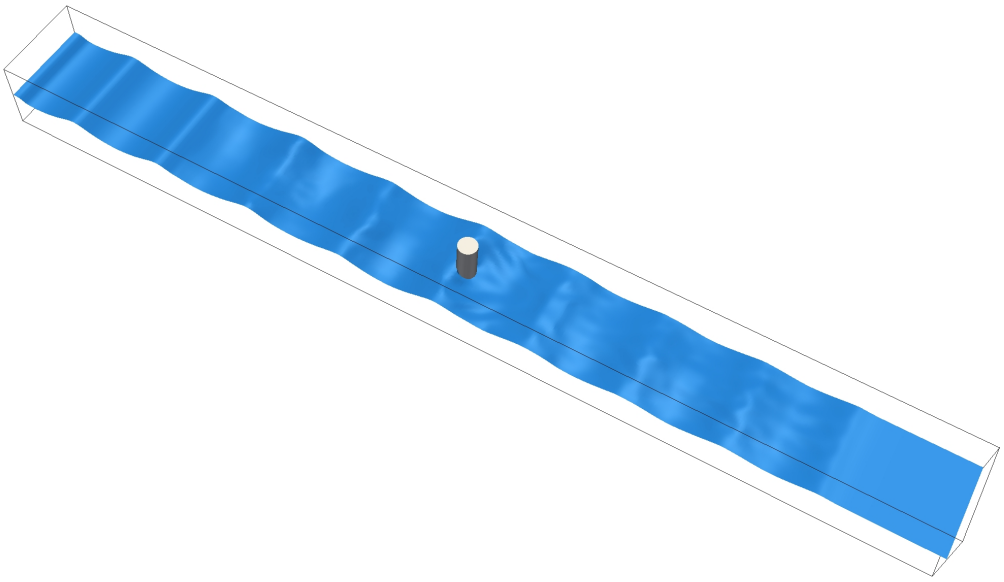

Figure 4.5: Detailed representation of the free surface: top view

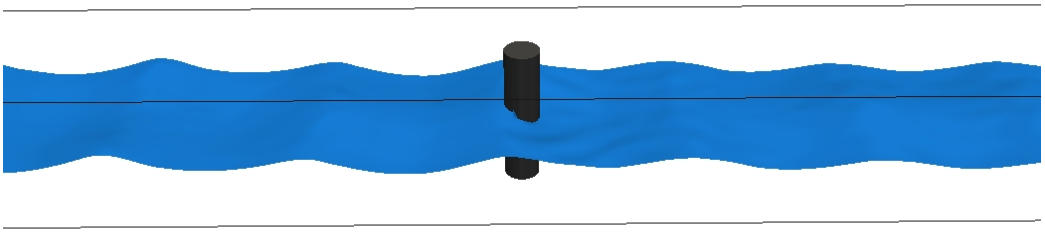

Figure 4.6: Detailed representation of the free surface: side view

The result for the second setup is shown in figure 4.10. The difference between the numerical and theoretical solution in this case is found to be marginally lower than the first setup at 23.9%. The slight reduction in the error may be reasoned as follows: The wavelength in this setup being $2.0m$, provides a higher grid density of 40 cells per wavelength. Again, using the conclusion from section 3.3.1, the reduced error can be justified. Also, in section 3.3.7, it has been reported that the wave tank seems to

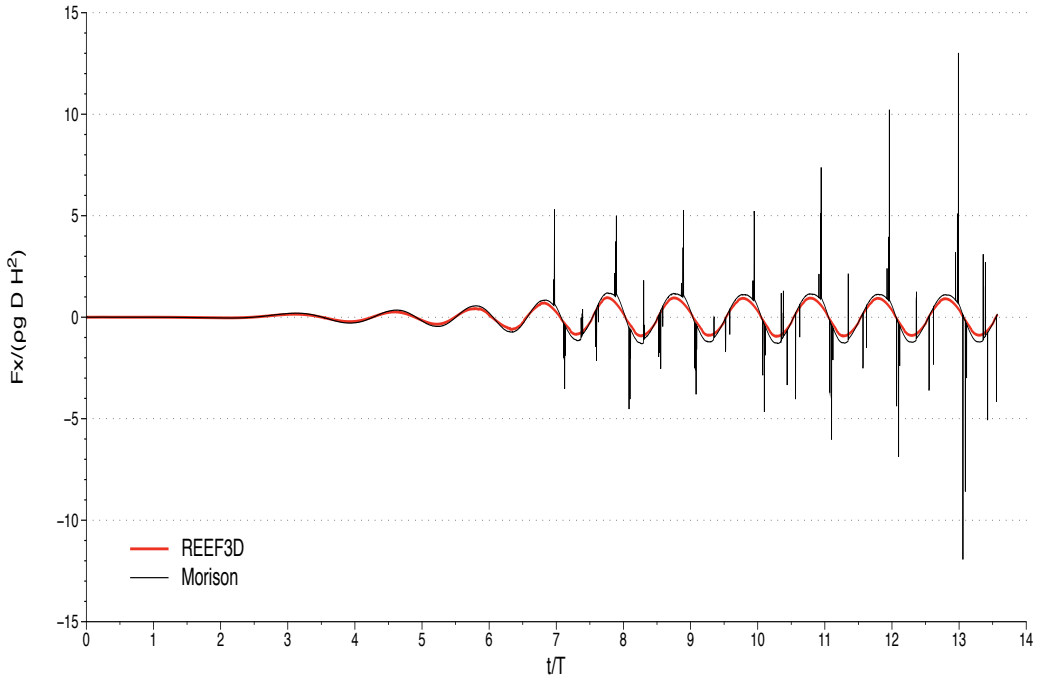

Figure 4.7: Unfiltered theoretical results and numerical results

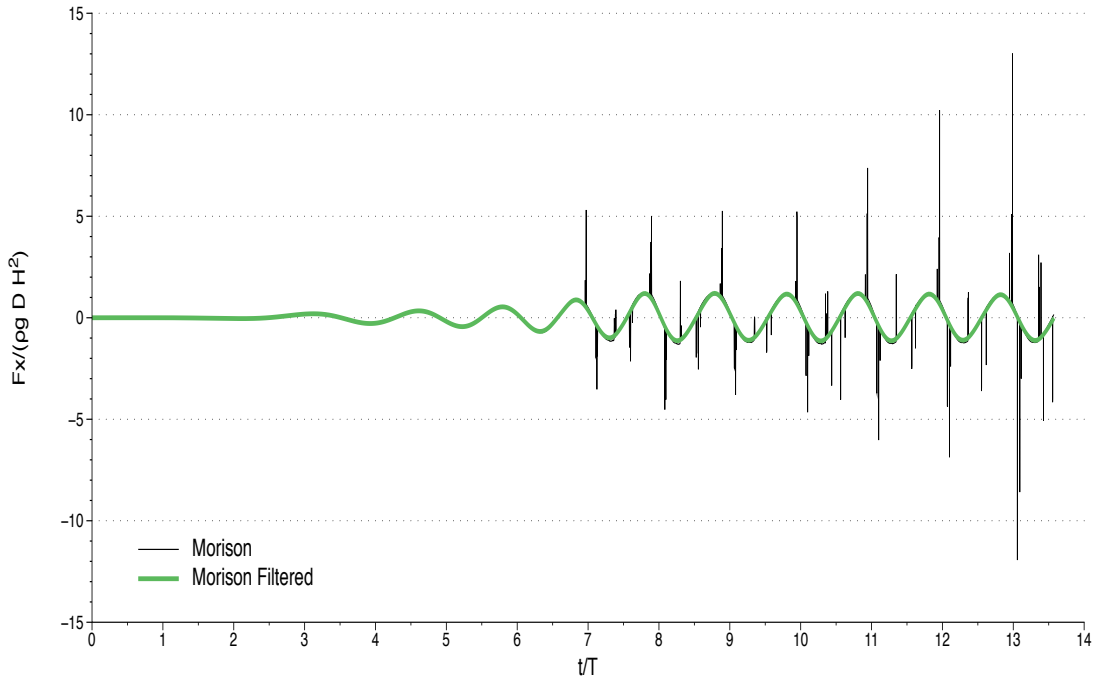

Figure 4.8: Filtering to smoothen theoretical results

perform better at higher amplitudes. This factor can also be attributed to the lower deviation of the numerical result from the theoretical value.

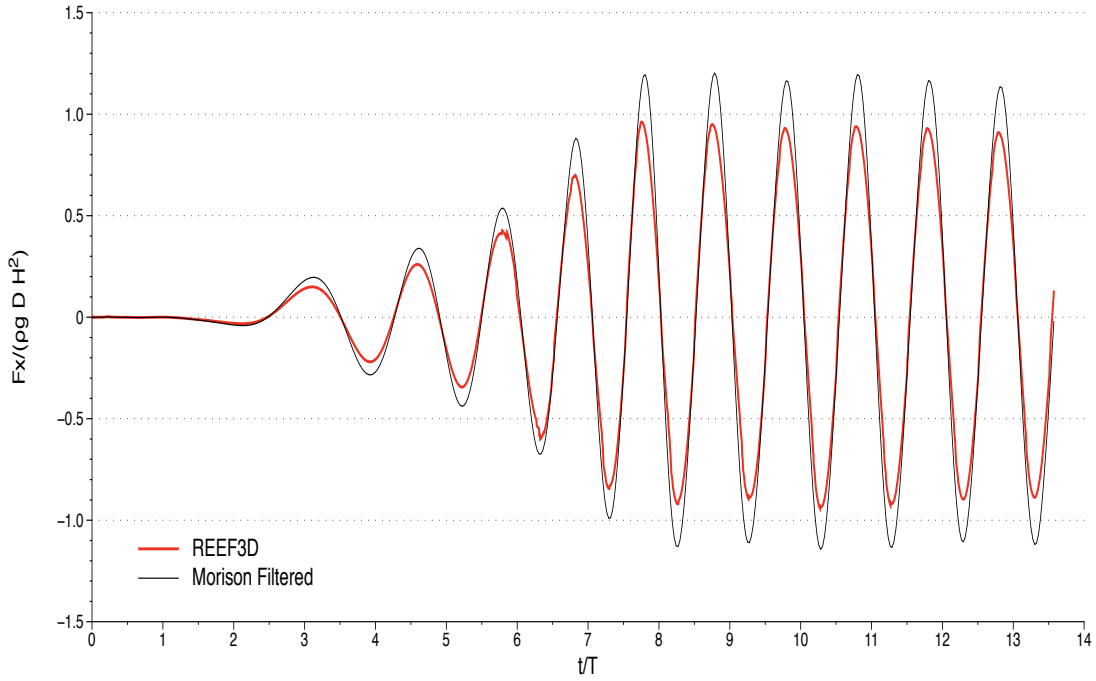

Figure 4.9: Comparison of numerical result with theory– Coarse grid, Setup 1

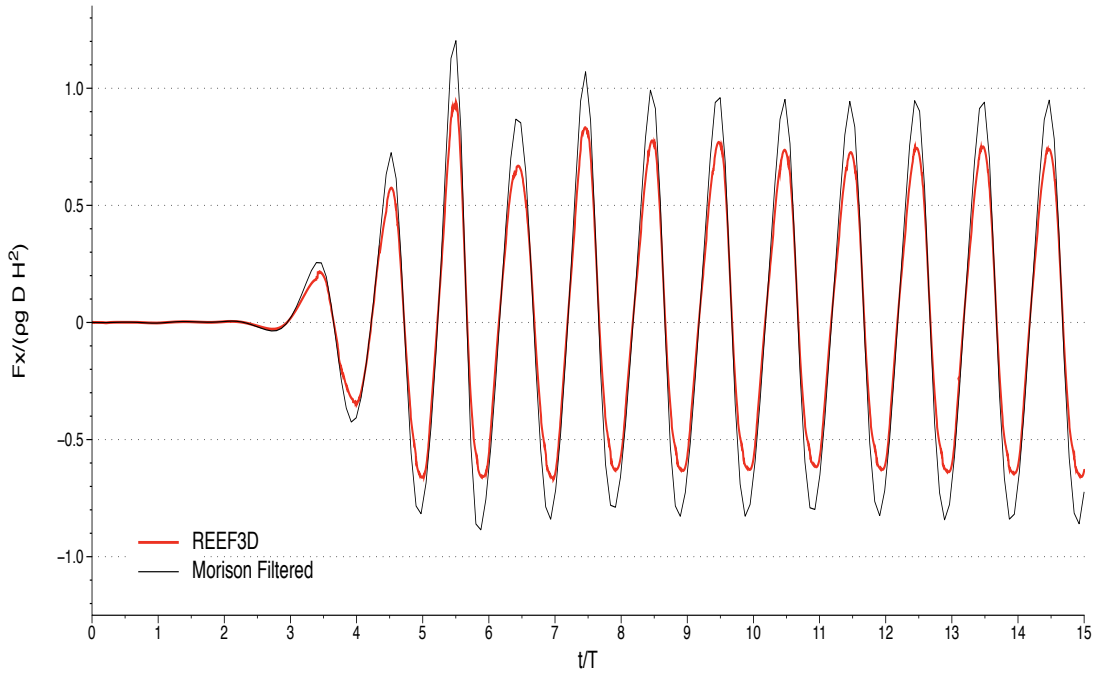

Figure 4.10: Comparison of numerical result with theory– Coarse grid, Setup 2

4.3.2 Fine grid experiments

The second set of numerical experiments is carried out on a finer grid with $dx = 0.025m$, that is, double the grid density compared to the first set. It is intuitively expected to obtain a better correlation of the numerical results at this grid resolution. Figure 4.11 displays the results obtained for the first setup. Contrary to expectations, the correlation between the numerical solution and the theoretical solution is seen to be lesser in this case. On an average, the deviation of the numerically resolved maximum force is lesser than the Morison force by 30%. The grid density in this trial is 40 cells per wavelength. The increased error observed here is hard to explain without further study.

The graph in figure 4.12 presents the results for the second setup. In this trial too, the numerically obtained maximum wave force is lesser than the theoretically calculated Morison force. But, it is interesting to note that the deviation in this case is the least of the four cases, with the difference being 22.7%. Intuitively, this case is expected to show the best results as it has the best grid cell density of 80 cells per wavelength. It is to be noted that the Morisonn force obtained on the finer grid is higher than the obtained on the coarser grid. The values of total force obtained for this grid configuration is higher for both REEF3D and Morison force compared to the coarse grid

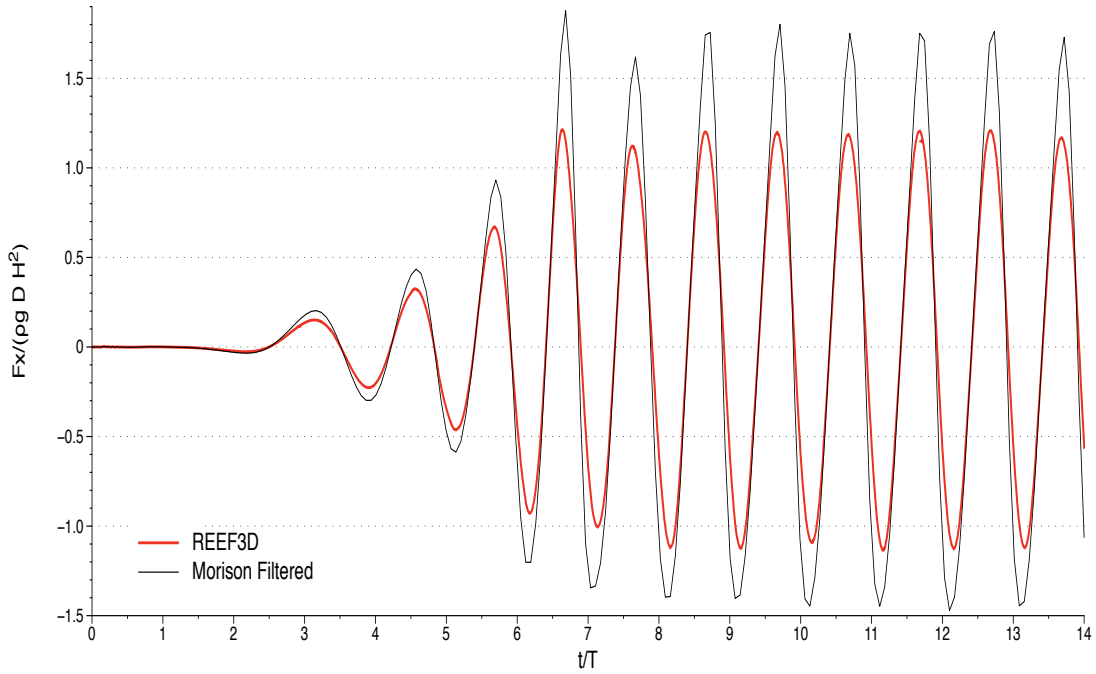

Figure 4.11: Comparison of numerical result with theory– Fine grid, Setup 1

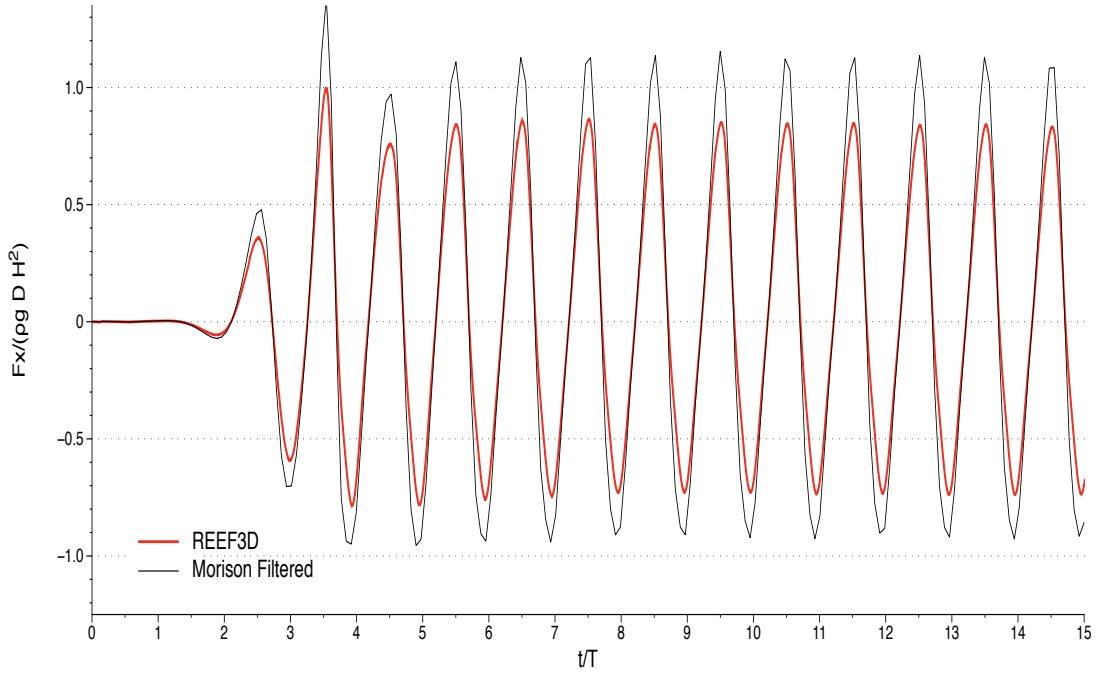

Figure 4.12: Comparison of numerical result with theory– Fine grid, Setup 2

Chapter 5

Conclusions and Outlook

5.1 Summary

Non-breaking wave forces on a cylindrical pile are calculated numerically by solving the three-dimensional Navier Stokes equations in the numerical wave tank of REEF3D. Initially, the numerical wave tank is validated by comparison of the numerical results with the analytical solutions for varying grid density, time step size, numerical beach width, wave amplitude, numerical methods− time and spatial discretization, relaxation method and wave type. The performance of the wave tank under the aforementioned various conditions is observed. As a result the appropriate parameters to be used for the numerical experiment are obtained. Finally, simulations are carried out to calculate the wave forces on a cylindrical pile and the numerical results are compared to the results obtained using the Morison formula.
During validation, it is observed that the wave tank gives good results with an error of 0.24% in the wave amplitude at a grid density of 100 cells per wavelength and CFL number 0.1 for a fifth order Stokes wave of amplitude $0.05m$ and wavelength $2m$. A recent study using a different approach reported a requirement of 200 cells per wavelength. Thus, the performance of the wave tank in this study is considered very good.
The calculation of wave forces also shows promising results. The wave forces from REEF3D seem to be slightly under estimated compared to the Morison force in the four numerical experiments carried out. There exists a possibility of erroneous calculation of the Morison force. There were no instabilities in the solution from the numerical calculations. Due to the absence of simple experimental data for wave force on a cylinder and time constraints, validation is attempted only through Morison formula by adding the formula in the code. The validation of wave force calculation could not be deemed conclusive.

5.2 Conclusions

The numerical wave tank in REEF3D is validated and utilized for calculation of wave forces on a cylindrical pile. Results from validation and performance testing of the wave tank are very promising. Wave amplitude error was restricted to 0.24% with a grid cell density of 100 cells per wavelength. In comparison to the study using OpenFOAM[1], which required a grid density of 200 to 400 cells, this result is encouraging as it signifies a reduced computational time for the simulation.
The 5^{th} order accurate WENO scheme is found to perform very well, without experiencing any numerical instability in the solution.
Performance of different wave types− fifth order Stokes, second order Stokes and linear waves are found to be satisfactory, with fifth order Stokes waves producing the best results. It can be safely concluded that REEF3D is well suited for simulating water waves.

The computational grid used in the model currently is a uniform Cartesian grid. Damping of smaller amplitude waves that is observed during the performance testing may be attributed to this feature, as the grid resolution along the y-axis can not be improved independent of the resolutions along the x and z axes. Also, use of specific grid resolution enhancement around regions of interest like the free surface and the vicinity of structures is not possible. Increasing the grid resolution uniformly all over the computational domain increases the number of computational cells by a large amount rendering the simulation inefficient.

The results obtained for the numerical experiments to calculate wave forces are summarized in table 5.1.

Table 5.1: Summary of numerical experiments

	Setup 1	Setup 2	dx
λ	$1.0m$	$2.0m$	
a	$0.05m$	$0.075m$	
d	$0.4m$	$0.4m$	
error(%)	25	23.9	$0.05m$
	30	22.7	$0.025m$

Looking at the configuration of the numerical experiments presented in table 5.1, it is logical to expect that, among the four cases presented,

- the trial with the combination of coarse grid and setup 1 will provide the worst results and

- the combination of fine grid and setup 2 will produce the best result.

But, from the results presented in section 4.3, the above logic is not completely followed. The best result are indeed from the second scenario. But the worst result is produced by the trial with setup 1, running on a fine grid. This casts some doubts over the calculation of the theoretical wave force. It is possible that the Morison formula is not evaluated correctly from the data taken from the simulation and hence gives rise to the anomaly in the results. This makes it difficult to effectively and conclusively validate the numerical solutions and discuss about the quality of numerical solution. In the absence of data from simple physical experiments for wave force on a cylinder and time constraints to numerically reproduce the experimental data presented in Mo et al.[22], the numerical experiment could not be validated against experimental data.
The fact that the numerical solution in the case with fine grid-setup 2 combination performs the best amongst the four, as expected, steers the conclusion that the mixed state of the results may not be a result of numerical calculations by REEF3D. Also, there is no numerical instability in the solutions produced.

5.3 Outlook

The testing of the numerical wave tank in REEF3D in this study has shown promising results. This study used the wave tank to simulate unidirectional regular waves to calculate non-breaking wave forces on a single cylindrical pile. The capabilities of the wave tank could be further explored, to enable simulation of scenarios with more complex wave-structure interactions. For example, generation of random waves using wave spectra like the JONSWAP spectrum and generation of multi-directional waves could be explored. Application of REEF3D to solve problems with complex hydrodynamics like wave interaction with floating structures seems to be an interesting area of research to expand the potential of the model.
Being a CFD program, REEF3D is resource intensive and effective over smaller temporal and spatial domains, compared to the popular tools in the field of marine civil engineering: wave models. In order to expand the reach of the program to deal with larger computational domains, the possibility of coupling the program with a Boussinesq wave model should be explored. With the integration of a wave model into the CFD code, wave generation, large regions of fetch and propagation can be covered by the wave model. The region of interest, where the fluid interaction phenomena have to be studied in more detail will be handled by the CFD code. This would result in an effective tool to cater to real world engineering problems.

With regard to implementing grid resolution enhancement at specific regions of interest, employing a multi-block grid would be a good addition to the program. A multi-block grid essentially means that grids with different grid sizes at various regions of the computational domain can be used in a simulation. This will result in more accurate and efficient computation by the use of a coarser grid for the general domain of the region and a fine grid in regions of special interest. Through this technique, parts of the wave tank, like the free surface and region of fluid interaction activity around structures can be monitored with a higher resolution grid providing a more detailed and accurate simulation.

Bibliography

[1] M. A. Afshar. Numerical wave generation in OpenFOAM. Master's thesis, Chalmers University of Technology, 2010.

[2] Ø. A. Arntsen and H. E. Krogstad. *Linear Wave Theory, Part A: Regular Waves*. Department of Civil and Transport Engineering, NTNU, Trondheim, 2000.

[3] P. A. Berthelsen and O. M. Faltinsen. A local directional ghost cell approach for incompressible viscous flow problems with irregular boundaries. *Journal of Computational Physics*, 227:4354–4397, 2008.

[4] H. Bihs. *Three Dimensional Numerical Modelling of Local Scour in Open Channel Flow*. PhD thesis, Norwegian University of Science and Technology, Trondheim, 2011.

[5] A. J. Chorin. Numerical solution of the Navier-Stokes equations. *Mathematics of Computation*, 22:745–762, 1968.

[6] G. F. Clauss, G. E. Schmittner, and R. Stück. Numerical wave tank- simulation of extreme waves for the investigation of structural responses. In *Proc., 24th International Conference on Offshore Mechanics and Arctic Engineering, Greece*, 2005.

[7] R. Courant, K. Friedrichs, and H. Lewy. On the partial difference equations of mathematical physics. *IBM Journal of Research and Development*, 11:215–234, 1967.

[8] R. G. Dean and R. A. Dalrymple. *Water Wave Mechanics for Engineers and Scientists*. World Scientific, 1991.

[9] A. P. Engsig-Karup. *Unstructured Nodal DG-FEM Solution of High-order Boussinesq-type Equations*. PhD thesis, Technical University of Denmark, Lyngby, 2006.

[10] J. D. Fenton. A fifth order stokes theory for steady waves. *Journal of Waterway, Port, Coastal and Ocean Engineering*, 111(2):216–234, 1985.

[11] J. H. Ferziger and M. Perić. *Computational Methods for Fluid Dynamics*. Springer-Verlag, 2002.

[12] P. H. Gaskell and A. K. C. Lau. Curvature-compensated convective transport:SMART, a new boundedness-preserving transport algorithm. *International Journal for Numerical Methods in Fluids*, 8:617–641, 1988.

[13] S. Grilli. Fully non linear potential flow models used for long wave run up prediction.

[14] A. Harten. High resolution schemes for hyperbolic conservation laws. *Journal of Computational Physics*, 49:357–393, 1983.

[15] L. Holthuijsen. *Waves in Oceanics and Coastal Waters*. Cambridge University Press, 2007.

[16] N. G. Jacobsen, D. Fuhrman, and J. Fredsøe. A wave generation toolbox for the open-source cfd library: Openfoam. *International Journal for Numerical Methods in Fluids*, 2011.

[17] G. S. Jiang and D. Peng. Weighted ENO schemes for Hamilton Jacobi equations. *SIAM Journal of Scientific Computing*, 21:2126–2143, 2000.

[18] S. K. Kim, P. L. Liu, and J. A. Liggett. Boundary integral equation solutions for solitary wave generation propagation and run-up. *Coastal Engineering*, 7:299–317, 1983.

[19] J. Larsen and H. Dancy. Open boundaries in short wave simulations-a new approach. *Coastal Engineering*, 7:285–297, 1983.

[20] X. D. Liu, S. Osher, and T. Chan. Weighted essentially non -oscillatory schemes. *Journal of Computational Physics*, 115:200–212, 1994.

[21] R. MacCamy and R. Fuchs. *Wave forces on piles: A diffraction theory*. University of California, Dept. of Engineering, 1954.

[22] W. Mo, K. Irschik, H. Oumeraci, and P. Liu. A 3D numerical model for computing non-breaking wave forces on slender piles. *Journal of Engineering Mathematics*, 58:19–30, 2007.

[23] G. Moe and O. Gudmestad. Predictions of morison type forces in irregular, high reynolds number waves. In *Proc., Seventh International Offshore and Polar Engineering Conference,Honolulu*, 1997.

[24] D. Peng, B. Merriman, S. Osher, H. Zhao, and M. Kang. A PDE-based fast local level set method. *Journal of Computational Physics*, 155:410–438, 1999.

[25] C. S. Peskin. Flow patterns around heart valves. *Journal of Computational Physics*, 10:252–271, 1972.

[26] T. Sarpkaya. *Wave Forces on Offshore Structures*. Cambridge University Press, 2010.

[27] H. Schlichting. *Boundary layer theory*. McGraw-Hill Book Company, 1979.

[28] C. Shu and S. Gottlieb. Total Variation Diminishing Range Kutta schemes. *Mathematics of Computation*, 67:73–85, 1998.

[29] B. M. Sumer and J. Fredsøe. *Hydrodynamics Around Cylindrical Structures*. World Scientific, 2006.

[30] M. Sussman, P. Smereka, and S. Osher. A level set approach for computing solutions to incompressible two-phase flow. *Journal of Computational Physics*, 114:146–159, 1994.

[31] Y. H. Tseng and J. H. Ferziger. A ghost-cell immersed boundary method for flow in complex geometry. *Journal of Computational Physics*, 192:593–623, 2003.

[32] H. A. van der Vorst. Bi-CGSTAB: A fast and smoothly converging variant of Bi-CG for the solution of nonsymmetric linear systems. *SIAM Journal on Scientific and Statistical Computing*, 13:631–644, 1992.

[33] B. van Leer. Towards the ultimate conservative difference scheme. *Journal of Computational Physics*, 32:101–136, 1979.

[34] D. C. Wilcox. *Turbulence Modeling for CFD*. DCW Industries Inc., La Canada, California., 1994.